Quantum Coherence in various Materials: Transparency, Harmonic Generation, Quantum Correlations, and Masers at Room Temperature

From gases to solids and living cells & From Classical fields to Quantum fields

Yuri Rostovtsev

Department of Physics and the Center for Nonlinear Sciences, University of North Texas, Denton, TX 76203 USA

Spectroscopy of materials can be enhanced by the quantum coherent effects. It is the quantum coherence effects such as electromagnetically induced transparency and coherent population trapping that attract attention due to the increasing development of new applications such as high-precision spectroscopy, and large Kerr nonlinearities. Localized plasmon interaction in quantum confined structures strongly modify the optical and electronic properties with potential for manipulating light on the nanoscale. Another approach to demonstrate quantum coherent and cooperative effects is to study the Bi-exponential decay of dye fluorescence near the surface of plasmonic metamaterials and core-shell nanoparticles that has been shown to be an intrinsic property of the coupled system.

We have demonstrated the new sensing mechanism based on an adiabatically changing electric field interacting with the rotational structure of the molecules with dipole moments. We have theoretically demonstrated a single low frequency gas detector that can be used for sensing of gas mixtures with high selectivity, accuracy, and sensitivity. The enhancement of the population difference between corresponding molecular levels and reached the theoretical maximum of absorption have been shown. Such a gas sensor can be used for a huge range of applications -- stretching from technology, sciences, control of environment, biology, and medicine.

Optica Laser Systems Technical Group, November 14, 2023

Outline

Motivation – what is quantum coherence? And why is it important?

Manipulation of population under interactions with adiabatically changing fields

Reduced graphene oxide and nanoparticles

- Electromagnetically induced transparency

Coherent effects in gases

- Gas sensing and masers at room temperature

Second harmonic generation in MoS2

Applications

- Generation of entanglement states,
  Application to quantum information and
  quantum processing and quantum sensing

Conclusion

A two-level atomic system

$$\hat{H} = \hbar\Delta|a\rangle\langle a| + \hbar\Omega(|a\rangle\langle b| + |b\rangle\langle a|)$$

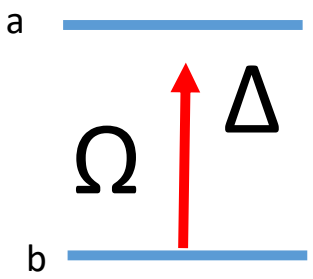

A two-level atomic system

$$\hat{H} = \hbar\Delta|a\rangle\langle a| + \hbar\Omega(|a\rangle\langle b| + |b\rangle\langle a|)$$

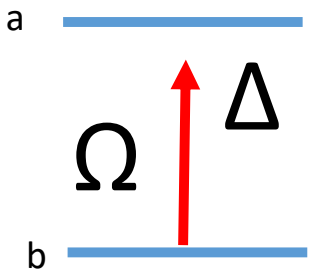

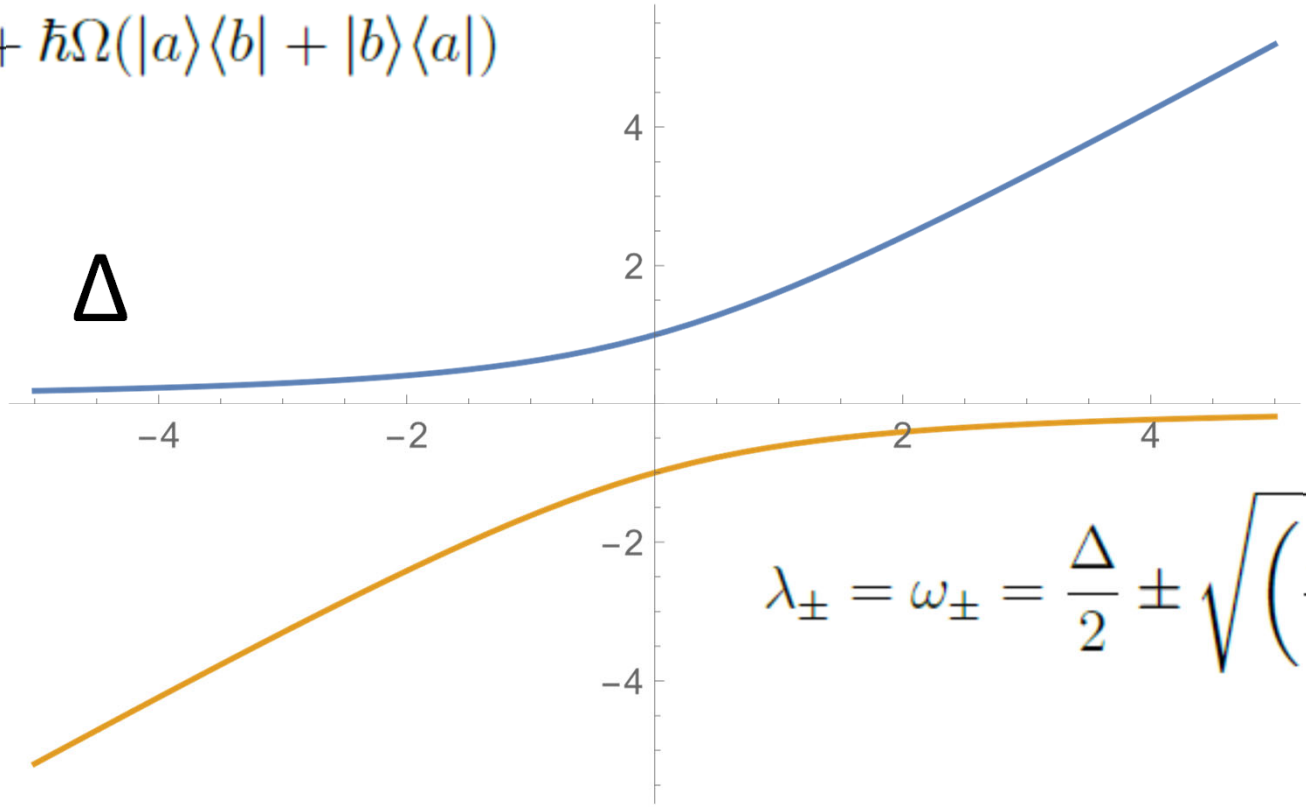

$$\lambda_{\pm} = \omega_{\pm} = \frac{\Delta}{2} \pm \sqrt{\left(\frac{\Delta}{2}\right)^2 + \Omega^2}$$

A two-level atomic system

$$\hat{H} = \hbar\Delta|a\rangle\langle a| + \hbar\Omega(|a\rangle\langle b| + |b\rangle\langle a|)$$

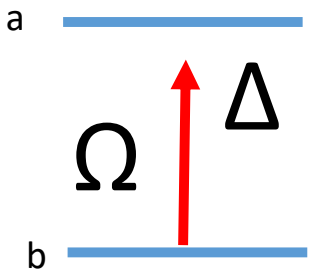

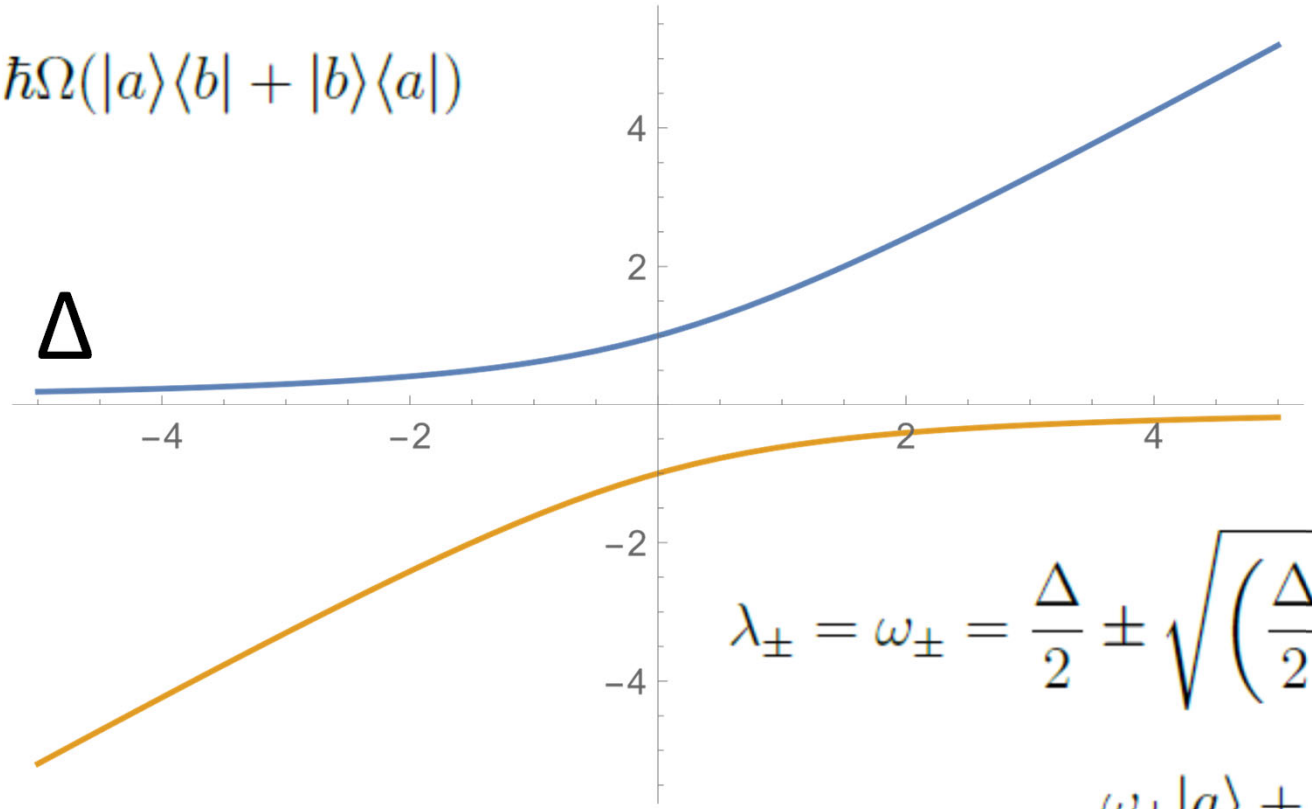

$$\lambda_\pm = \omega_\pm = \frac{\Delta}{2} \pm \sqrt{\left(\frac{\Delta}{2}\right)^2 + \Omega^2}$$

$$|\pm\rangle = \frac{\omega_\pm|a\rangle + \Omega|b\rangle}{\sqrt{\omega_\pm^2 + \Omega^2}}$$

CHIRAP in a two-level atomic system

$$\hat{H} = \hbar\Delta|a\rangle\langle a| + \hbar\Omega(|a\rangle\langle b| + |b\rangle\langle a|)$$

$$\lambda_{\pm} = \omega_{\pm} = \frac{\Delta}{2} \pm \sqrt{\left(\frac{\Delta}{2}\right)^2 + \Omega^2}$$

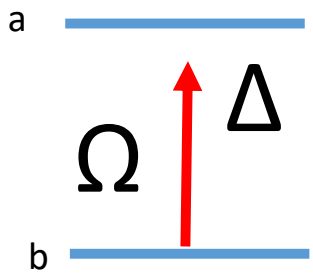

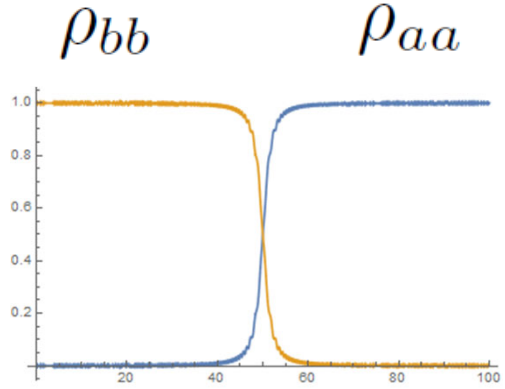

$$\omega_+(\Delta) = \begin{cases} 0, & \Delta \to -\infty \\ \Delta, & \Delta \to +\infty \end{cases} \quad \text{and} \quad |+\rangle(\Delta) = \begin{cases} |b\rangle, & \Delta \to -\infty \\ |a\rangle, & \Delta \to +\infty \end{cases}$$

$$\omega_-(\Delta) = \begin{cases} \Delta, & \Delta \to -\infty \\ 0, & \Delta \to +\infty \end{cases} \quad \text{and} \quad |-\rangle(\Delta) = \begin{cases} |a\rangle, & \Delta \to -\infty \\ |b\rangle, & \Delta \to +\infty \end{cases}$$

[1] Selective excitation of diatomic molecules by chirped laser pulses, J. Chem. Phys. 113, 4901 (2000); Bo Y. Chang *and* Ignacio R. Solá, Vladimir S. Malinovsky, Jesús Santamaría;

[2] Adiabatic Passage Control Methods for Ultracold Alkali Atoms and Molecules via Chirped Laser Pulses and Optical Frequency Combs, SA Malinovskaya, G Liu, Advances in Quantum Chemistry 77, 241-294 (2018).

$$\hat{H} = \hbar\Omega_p |b\rangle\langle a| + \text{adj}$$

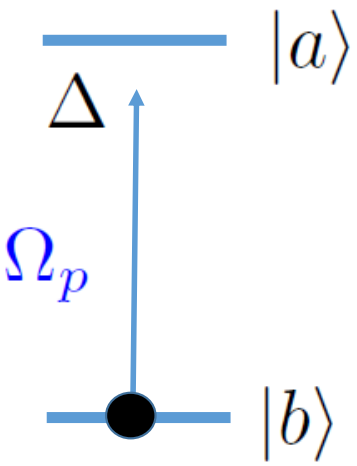

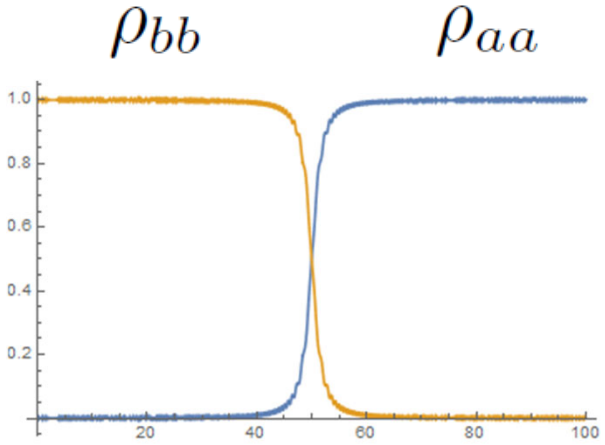

$$\Delta = \Delta_0 - \alpha t$$

$$\hat{H} = \hbar\Omega_p|b\rangle\langle a| + \text{adj}$$

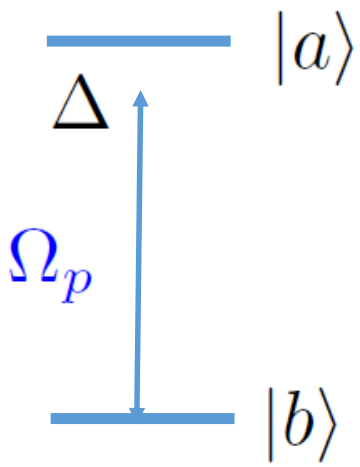

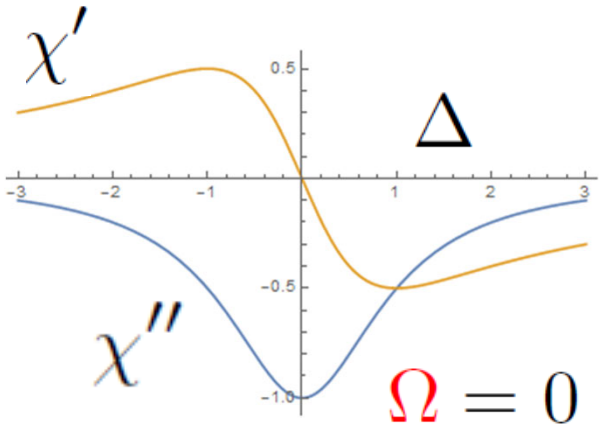

$$\hat{H} = \hbar\Omega_p|b\rangle\langle a| + \text{adj}$$

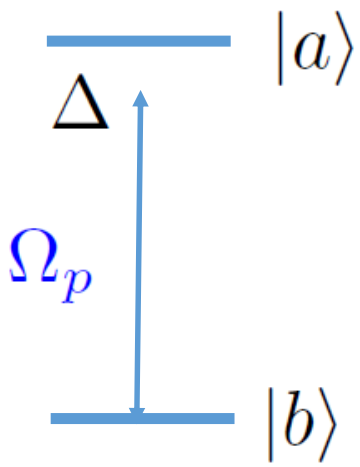

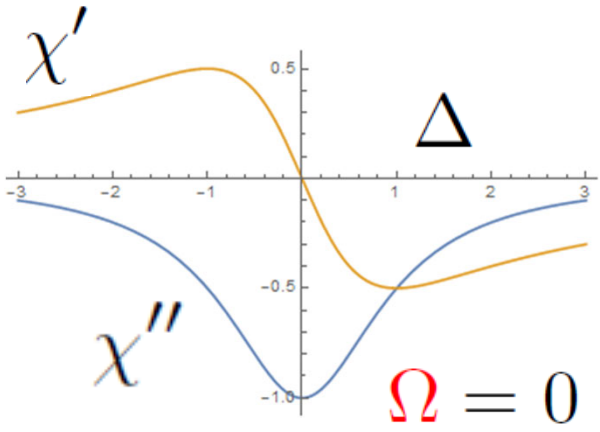

$$\hat{H} = \hbar(\Omega_p|b\rangle\langle a| + \Omega|c\rangle\langle a|) + \text{adj}$$

$$|B\rangle = \frac{\Omega_p|b\rangle + \Omega|c\rangle)}{\sqrt{|\Omega|^2 + |\Omega_p|^2}}$$

$$|D\rangle = \frac{\Omega|b\rangle - \Omega_p|c\rangle)}{\sqrt{|\Omega|^2 + |\Omega_p|^2}}$$

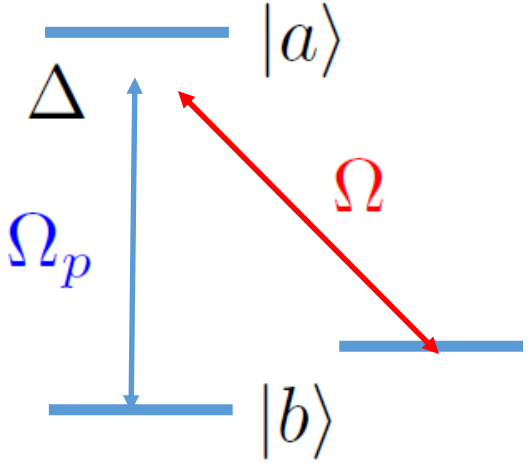

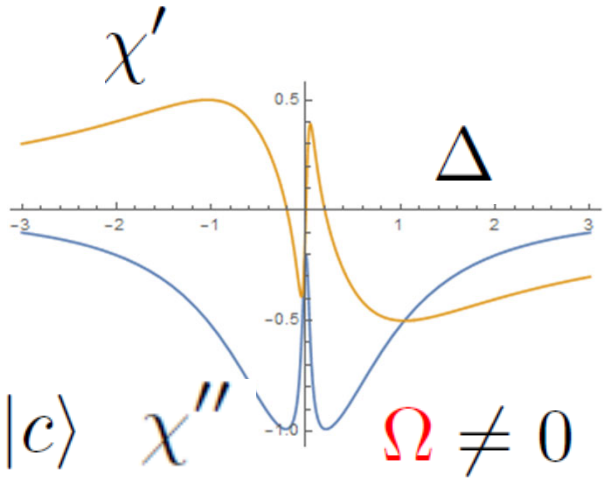

$$\hat{H} = \hbar(\Omega_p|b\rangle\langle a| + \Omega|c\rangle\langle a|) + \text{adj}$$

$$|B\rangle = \frac{\Omega_p|b\rangle + \Omega|c\rangle)}{\sqrt{|\Omega|^2 + |\Omega_p|^2}}$$

$$|D\rangle = \frac{\Omega|b\rangle - \Omega_p|c\rangle)}{\sqrt{|\Omega|^2 + |\Omega_p|^2}}$$

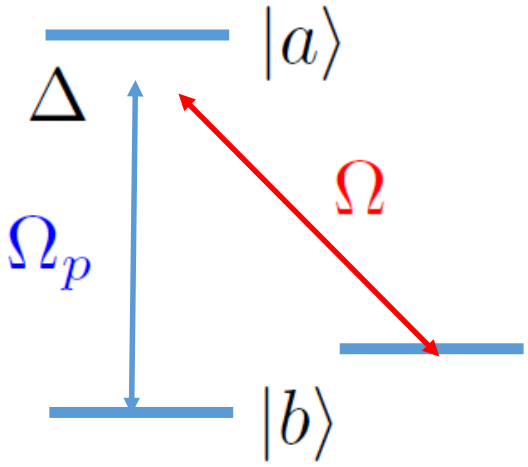

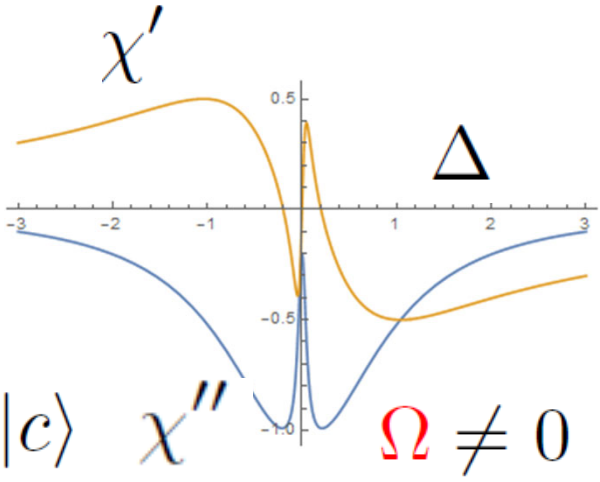

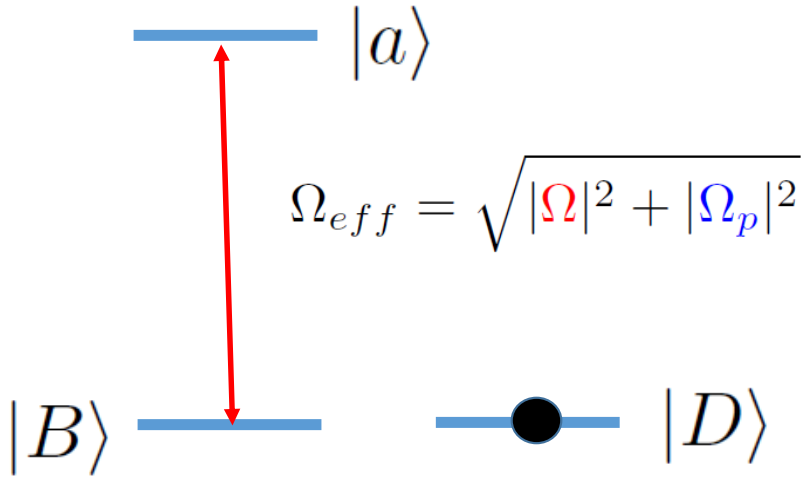

$$\hat{H} = \hbar(\Omega_p|b\rangle\langle a| + \Omega|c\rangle\langle a|) + \text{adj}$$

$$|B\rangle = \frac{\Omega_p|b\rangle + \Omega|c\rangle)}{\sqrt{|\Omega|^2 + |\Omega_p|^2}}$$

$$|D\rangle = \frac{\Omega|b\rangle - \Omega_p|c\rangle)}{\sqrt{|\Omega|^2 + |\Omega_p|^2}}$$

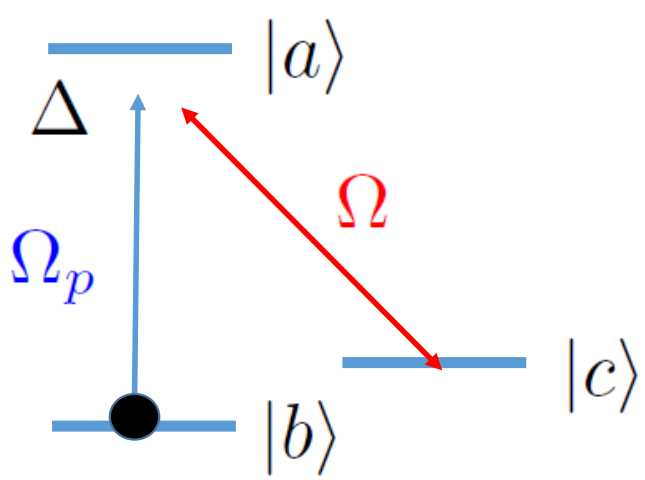

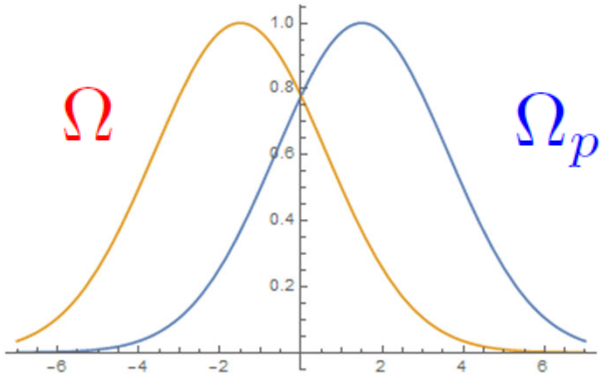

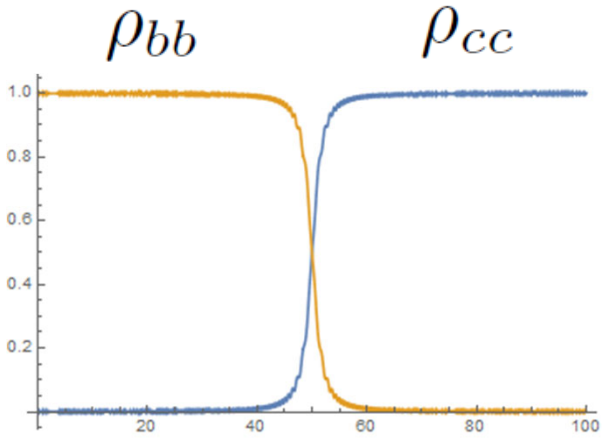

Electromagnetically Induced Transparency in gases

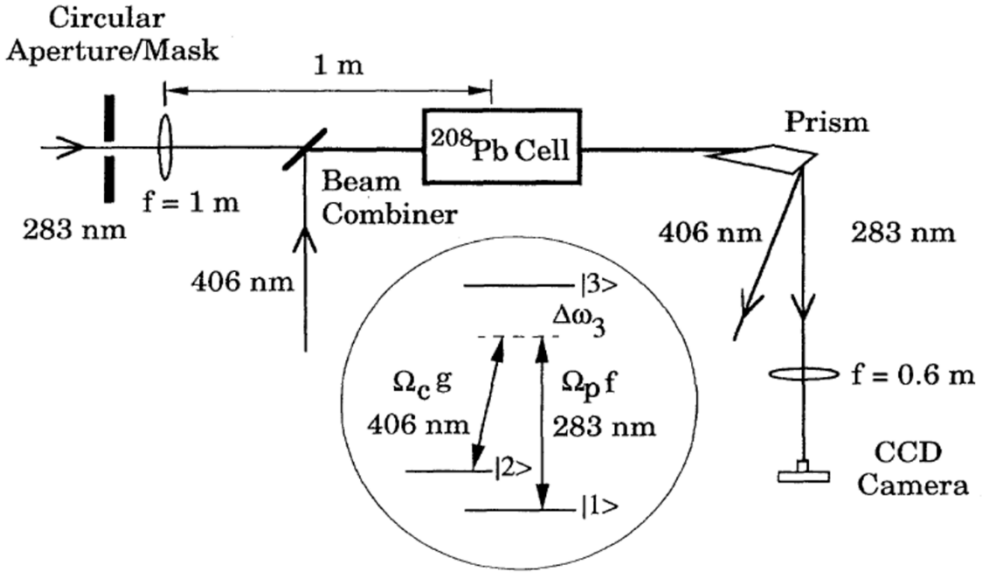

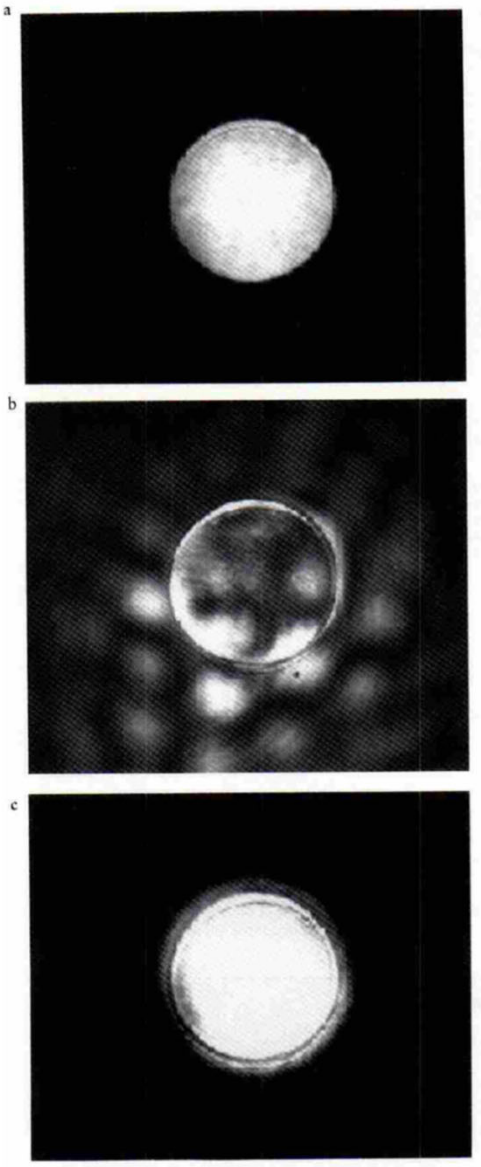

A. Kasapi, M. Jain, G. Y. Yin, and S. E. Harris, Electromagnetically Induced Transparency: Propagation Dynamics, Phys. Rev. Lett. **74**, 2447 – Published 27 March 1995

M. Jain, A. J. Merriam, A. Kasapi, G. Y. Yin, and S. E. Harris, Elimination of Optical Self-Focusing by Population Trapping, Phys. Rev. Lett. **75**, 4385 (1995)

Electromagnetically Induced Transparency in gases: applications

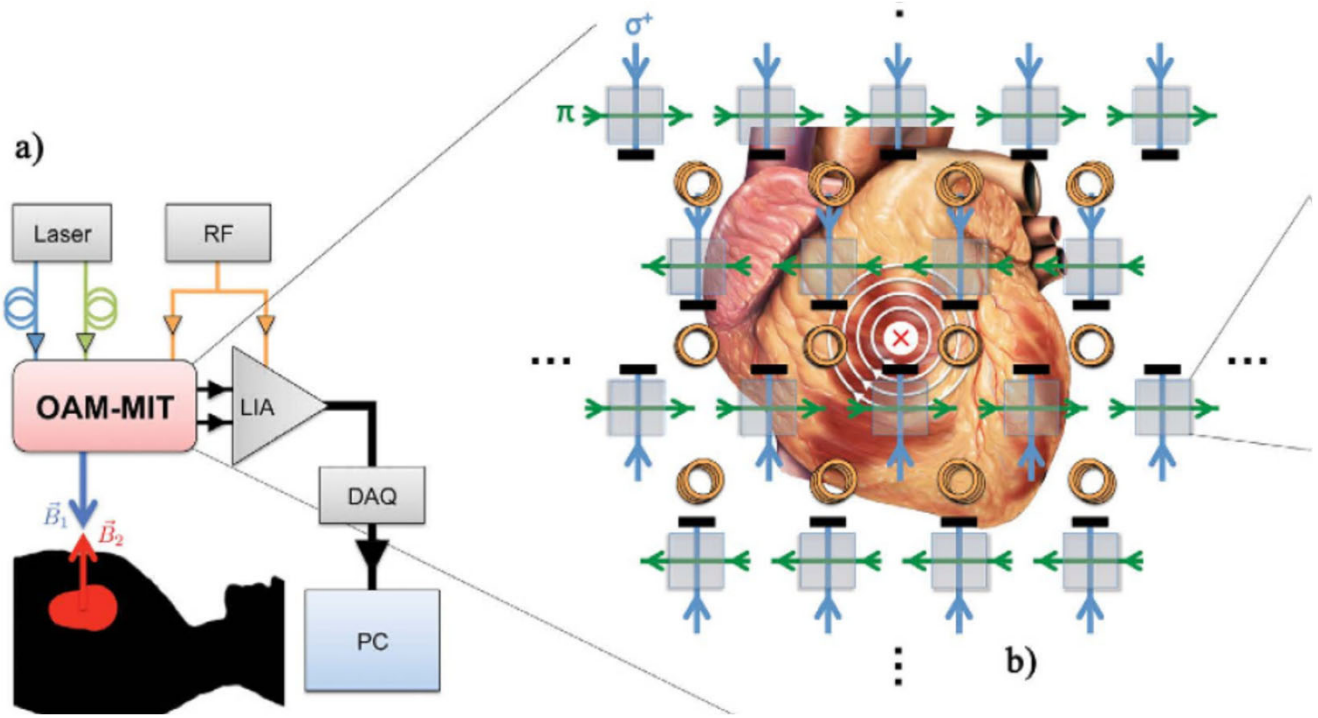

Marmugi, L., Renzoni, F. Optical Magnetic Induction Tomography of the Heart. *Sci Rep* **6,** 23962 (2016). https://doi.org/10.1038/srep23962

Electromagnetically Induced Transparency in gases: applications

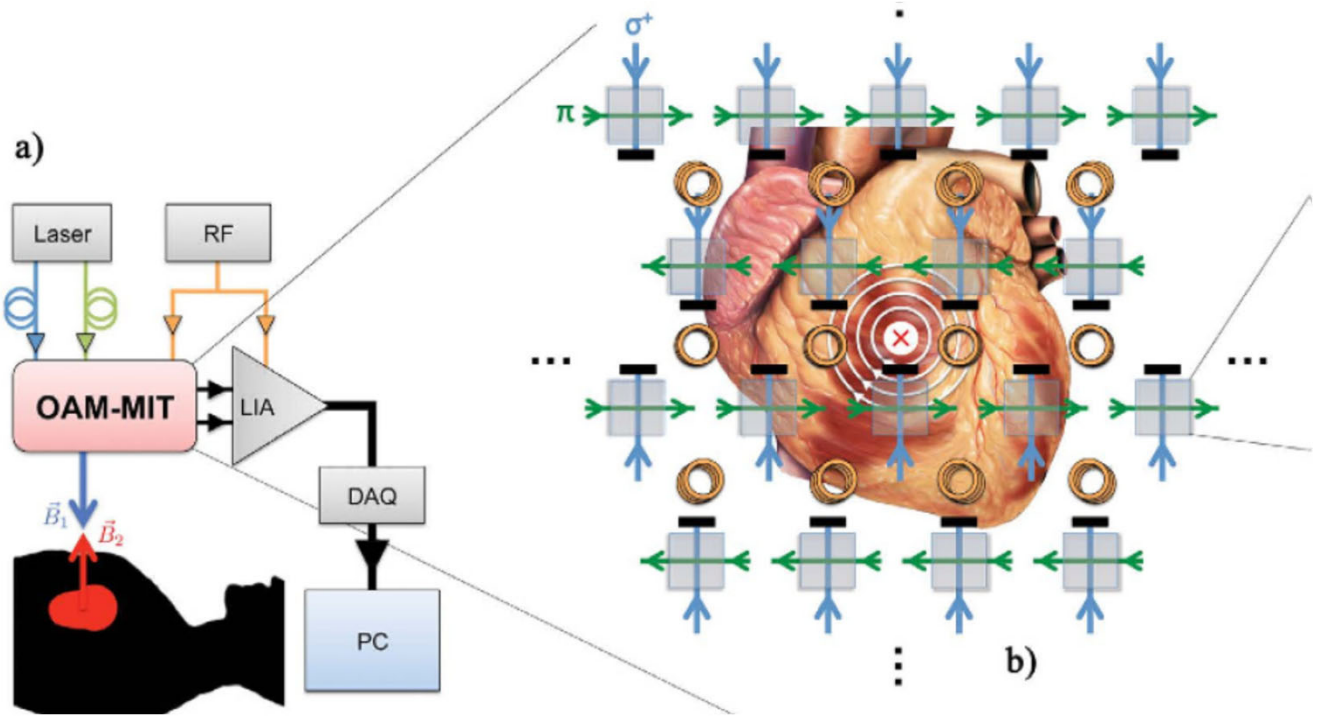

Marmugi, L., Renzoni, F. Optical Magnetic Induction Tomography of the Heart. *Sci Rep* **6,** 23962 (2016). https://doi.org/10.1038/srep23962

Pump-Probe Spectroscopy

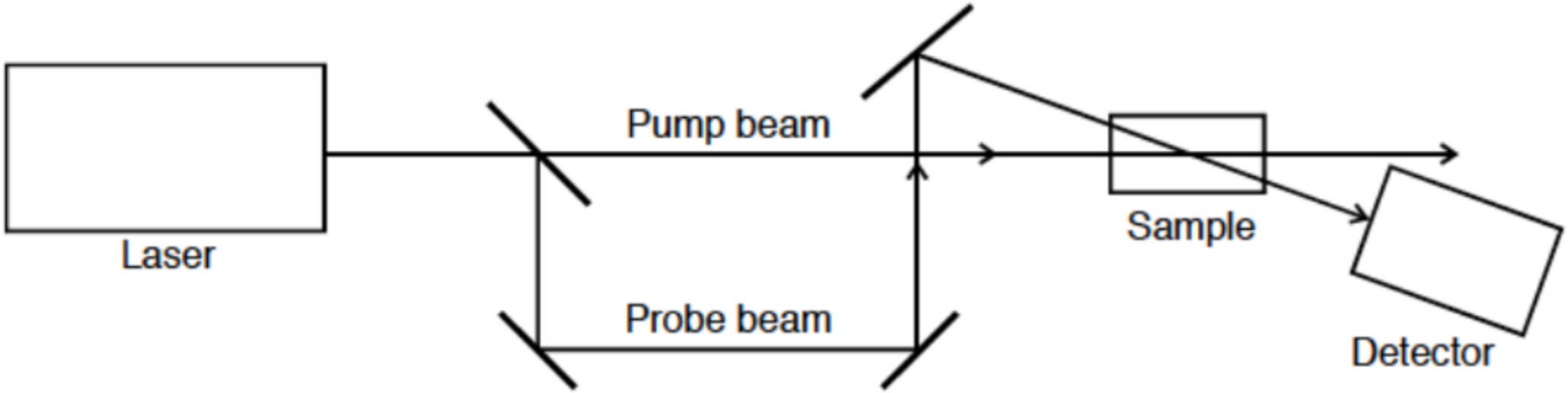

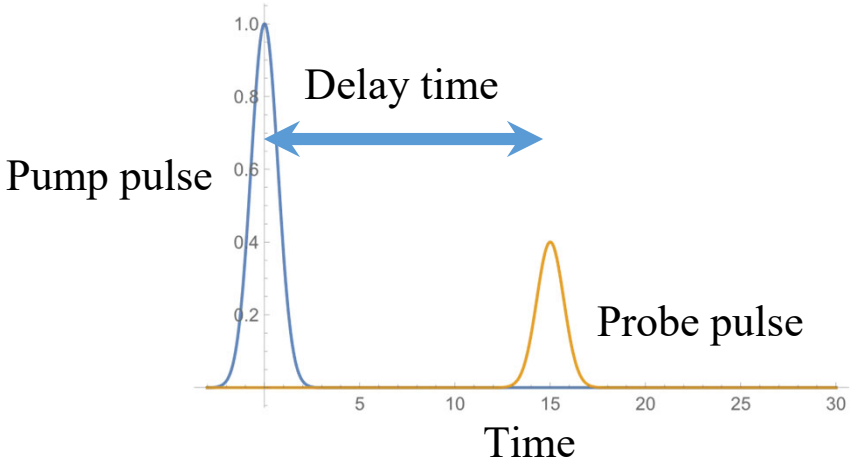

Reduced graphene oxide and nanoparticles

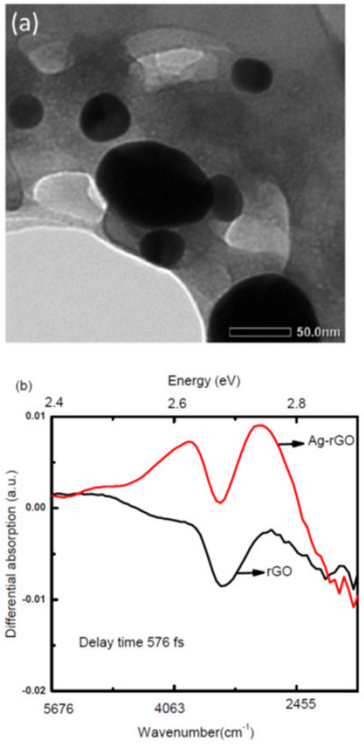

FIG. 1. (a) High resolution HRTEM image of Ag NPs on thin sheet of rGO. The size of NPs is chosen so that LSP of Ag NPs are close to the emission of rGO. (b) The differential absorption spectrum of rGO and Ag-rGO for the delay time between the pump and probe laser pulses of 576 fs.

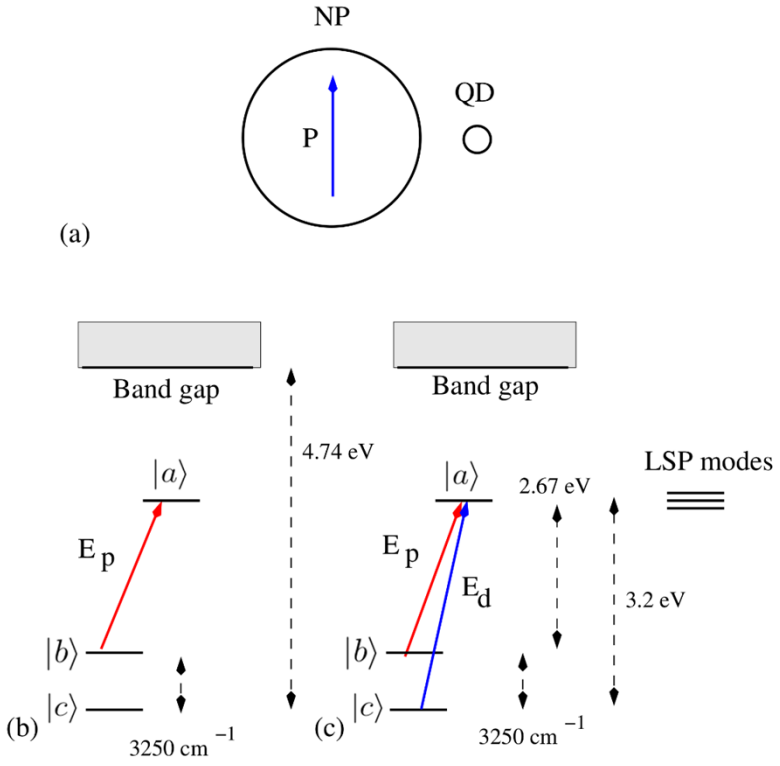

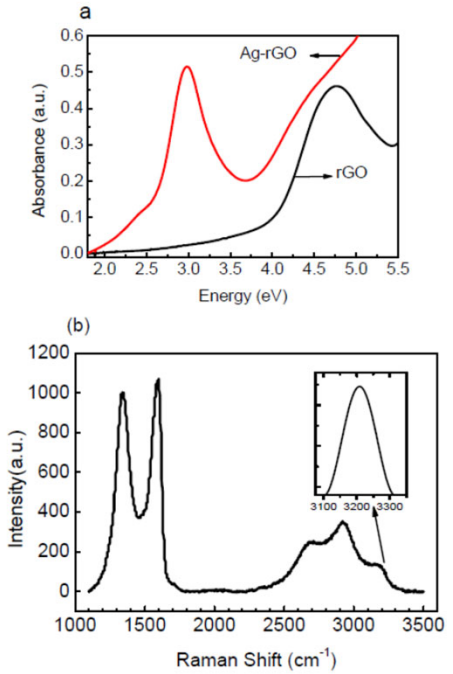

FIG. 3. (a) UV-vis absorption of rGO with and without Ag-NPs. (b) Raman spectra of rGO obtained by using a 532 nm laser excitation. The inset shows the Raman scattering that related to 3250 wavenumber phonon scattering.

Meg Mahat, Yuri Rostovtsev, Sanjay Karna, Gary N Lim, Francis D'Souza, Arup Neogi, Plasmonically induced transparency in graphene oxide quantum dots with dressed phonon states, *ACS Photonics*, **2017**, 5, 614-62

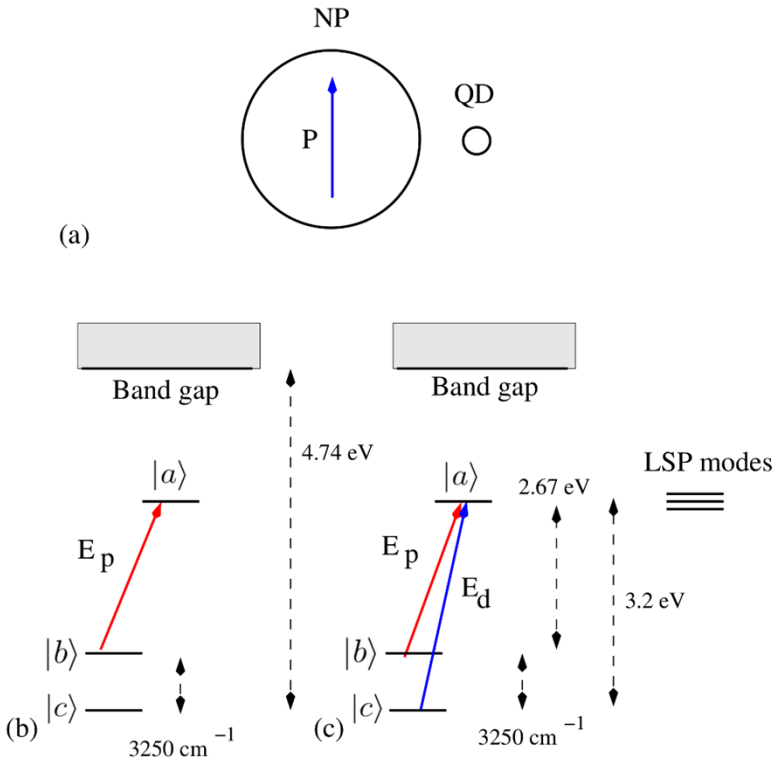
NP
QD
P
(a)
Band gap
Band gap
4.74 eV
LSP modes
$|a\rangle$
E p
$|b\rangle$
$|c\rangle$
(b)
3250 cm −1
$|a\rangle$
2.67 eV
E p
E d
3.2 eV
$|b\rangle$
$|c\rangle$
(c)
3250 cm −1

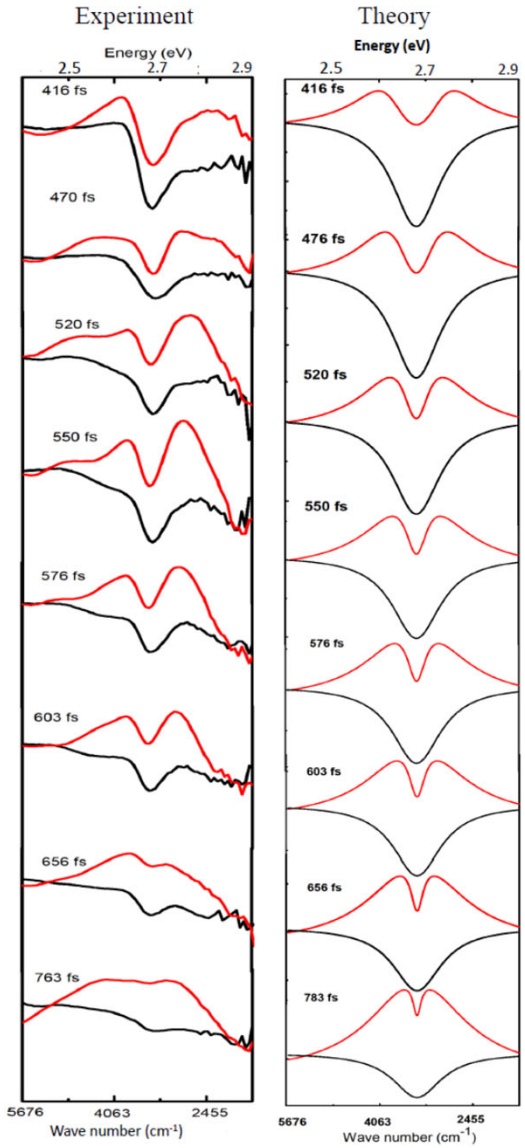
Experiment
Theory
Energy (eV)
2.5
2.7
2.9
416 fs
470 fs
520 fs
550 fs
576 fs
603 fs
656 fs
763 fs
476 fs
783 fs
5676
4063
2455
Wave number (cm-1)

Coherent effects for sensing and detecting

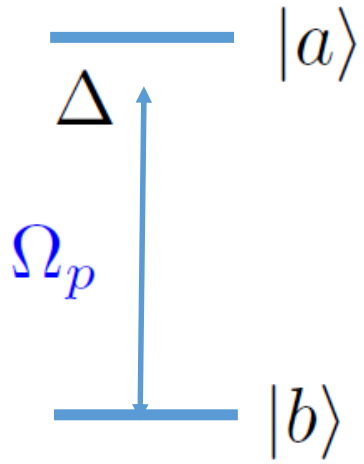

(A) Not coherent

$$\rho_{aa} = \frac{2|\Omega_p|^2}{\gamma^2 + \Delta^2 + 2|\Omega_p|^2}\rho_{bb}$$

$$P_{|b\rangle \to |a\rangle} \leq 50\%$$

(B) Coherent

$$P_{|b\rangle \to |a\rangle} = 100\%$$

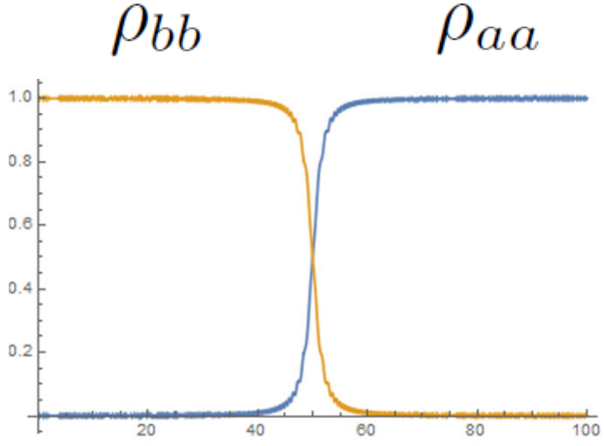

Z Branković, Y Rostovtsev, A resonant single frequency molecular detector with high sensitivity and selectivity for gas mixtures, Scientific Reports 10, 1537 (2020)

Sensing molecules with electric dipole

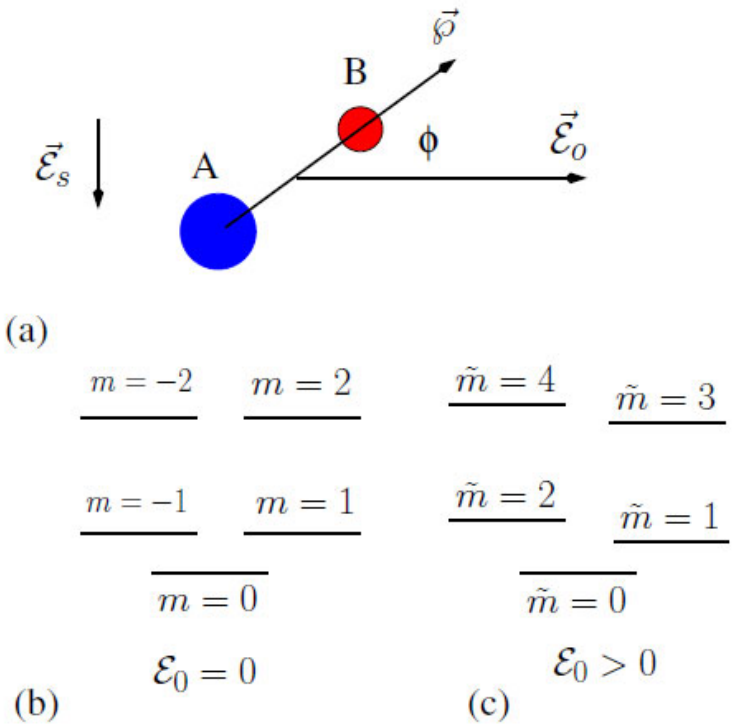

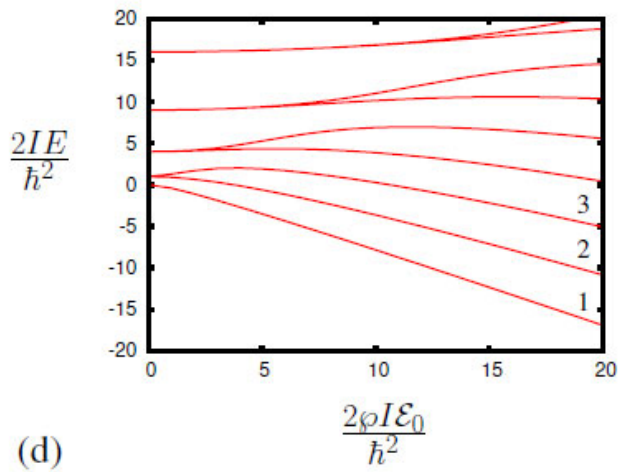

M. Lemeshko, et al., Manipulation of molecules with electromagnetic fields, MOLECULAR PHYSICS 111, 1648-1682 (2013).

H.J. Loesch, J. Bulthuis, S. Stolte, A. Durand, J.-C. Loison, J. Vigu´e, Molecules Oriented by Brute Force, Europhysics News 27, 12-15 (1996).

$$\hat{H} = B\hat{J}_z^2 - \vec{\wp}\cdot\vec{\mathcal{E}}_0 \qquad \hat{H} = -\frac{\hbar^2}{2I}\frac{\partial^2}{\partial\phi^2} + \frac{I\omega_E^2}{2}\phi^2 - \wp\mathcal{E}_0$$

Molecular alignment $\hbar\omega_E \gg k_B T$ $\qquad \wp\mathcal{E}_0 \gg \left(\frac{k_B T}{\hbar B}\right)^2 \hbar B$ $\qquad \omega_E^2 = \frac{\wp\mathcal{E}_0}{I}$

Weak alignment $\wp\mathcal{E}_0 \simeq \hbar B,$

Cavity

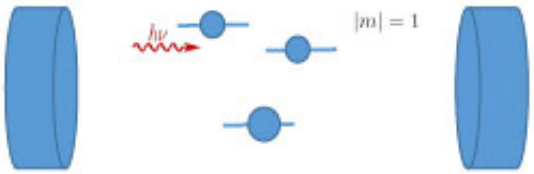

$$\dot{\Omega}_s = -i(\omega_0 - \omega_s)\Omega_s + i\Omega_a^2\rho_{ab}$$

$$\Omega_a^2 = \frac{2\pi\omega_0\wp^2 N}{\hbar}$$

$$i\hbar\dot{\rho} = [\hat{H}, \rho].$$

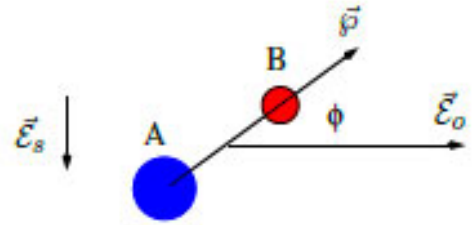

(a)

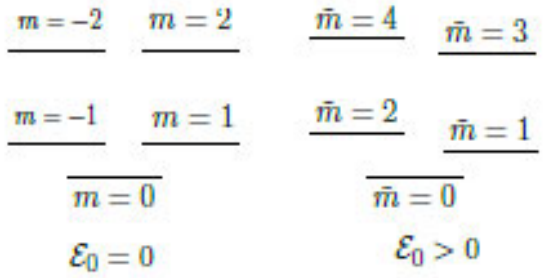

(b) (c)

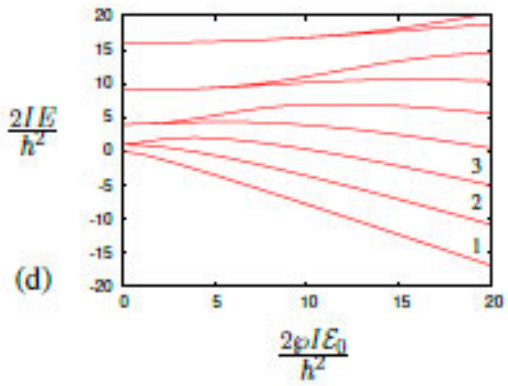

(d)

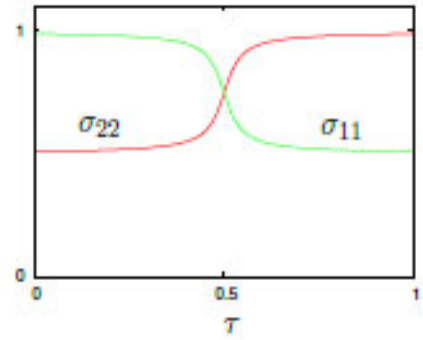

(e)

Cavity

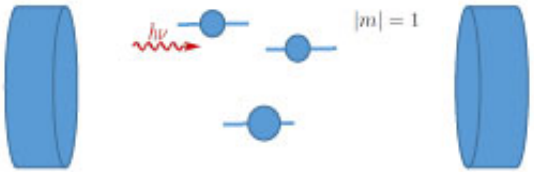

$$\frac{2I(E_2 - E_1)}{\hbar^2} = F\left(\frac{2\wp I\mathcal{E}_0}{\hbar^2}\right)$$

$$\delta\Theta \simeq \frac{\delta P_s}{P_s} = \frac{P_{noise}}{P_s}$$

$$\delta N_{min} = \frac{\hbar\alpha}{2\pi\omega_0\wp^2}\frac{P_{noise}}{P_s}$$

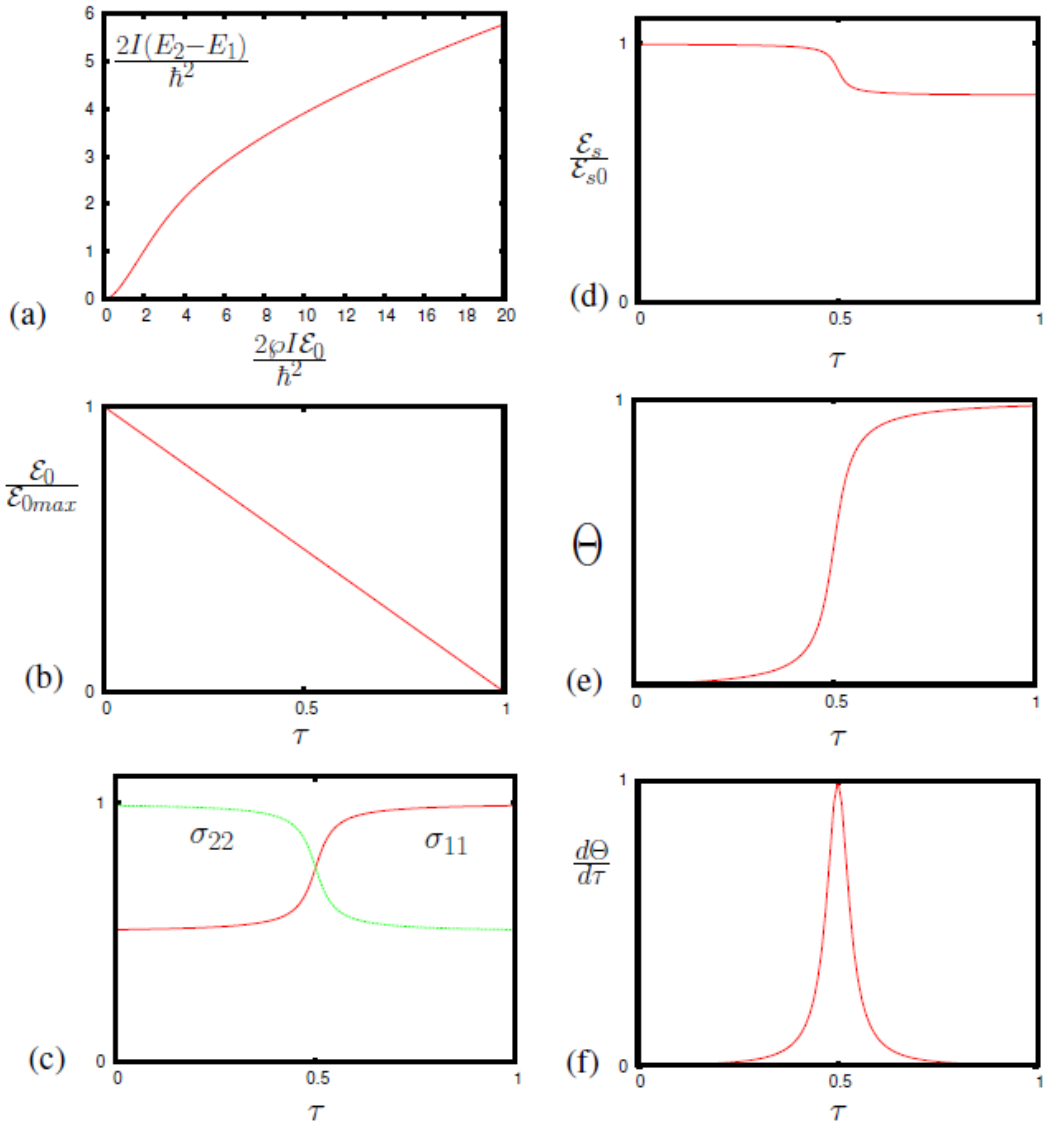

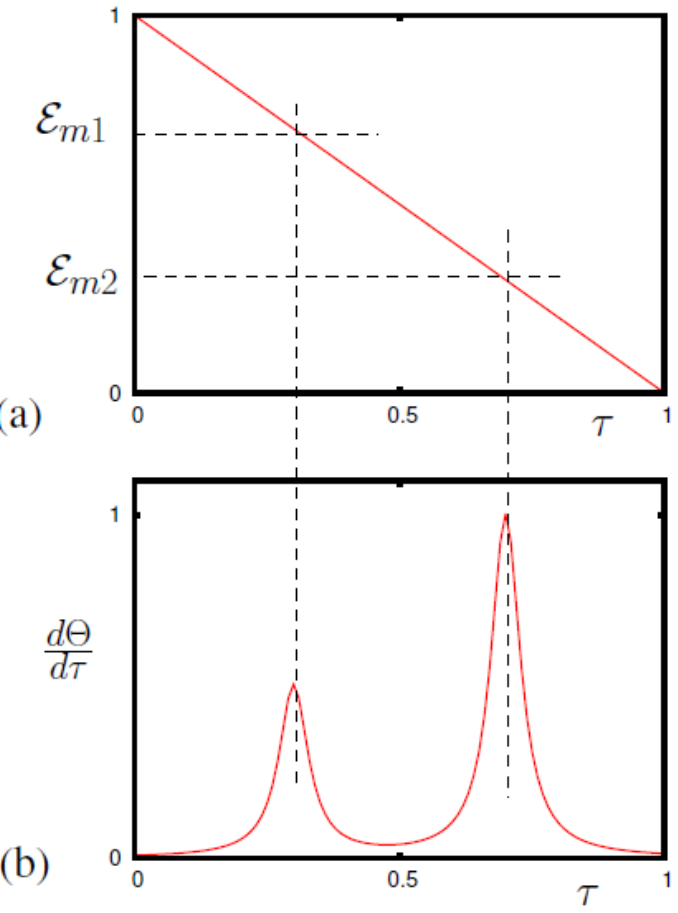

Molecules	Dipole	Rotational Constant	dc Electric field	Minimum density
CO,	$\wp_{CO} = 0.122$ D,	$B = 1.93$ cm^{-1};	45 10^3 V/cm,	2 10^{10} cm^{-3}
HCN,	$\wp_{HCN} = 2.98$ D,	$B = 1.47$ cm^{-1},	1600 V/cm,	3 10^{10} cm^{-3}
N_2O,	$\wp_{N_2O} = 0.17$ D,	$B = 0.42$ cm^{-1};	15 10^3 V/cm,	9 10^{10} cm^{-3}
NO,	$\wp_{NO} = 0.16$ D,	$B = 1.67$ cm^{-1},	30 10^3 V/cm,	2 10^{10} cm^{-3}
SO,	$\wp_{SO} = 1.55$ D,	$B = 0.72$ cm^{-1},	2200 V/cm,	5 10^{10} cm^{-3}
KBr,	$\wp_{KBr} = 10.6$ D,	$B = 0.08$ cm^{-1},	106 V/cm,	5 10^9 cm^{-3}
NO_2,	$\wp_{NO_2} = 0.316$ D,	$A = 8.0$ cm^{-1},	8300 V/cm,	9 10^{10} cm^{-3}
		$B = 0.43$ cm^{-1},		
		$C = 0.41$ cm^{-1},		
H_2O,	$\wp_{H_2O} = 1.85$ D,	$A = 27.88$ cm^{-1},	6500 V/cm,	4 10^9 cm^{-3}
		$B = 14.512$ cm^{-1},		
		$C = 9.29$ cm^{-1},		
O_3,	$\wp_{O_3} = 0.53$ D,	$A = 3.550$ cm^{-1},	4800 V/cm,	1 10^{11} cm^{-3}
		$B = 0.44$ cm^{-1},		
		$C = 0.39$ cm^{-1},		
CCl_2O,	$\wp_{CCl2O} = 1.17$ D,	$A = 0.26$ cm^{-1},	1080 V/cm,	4 10^{11} cm^{-3}
		$B = 0.16$ cm^{-1},		
		$C = 0.08$ cm^{-1},		
NH_3,	$\wp_{NH_3} = 1.47$ D,	$A = 9.44$ cm^{-1},	6600 V/cm,	6 10^9 cm^{-3}
		$B = 9.44$ cm^{-1},		
		$C = 6.19$ cm^{-1},		

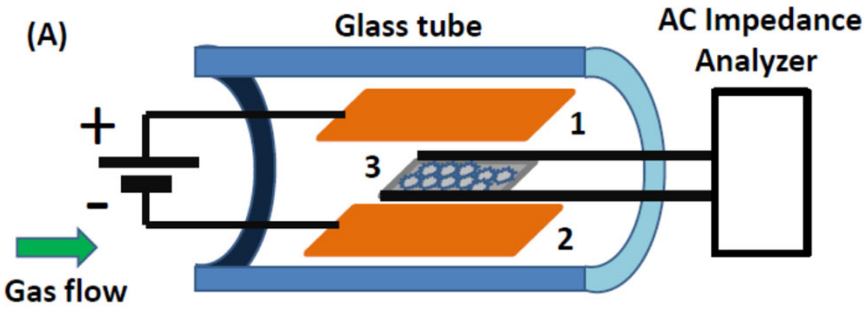

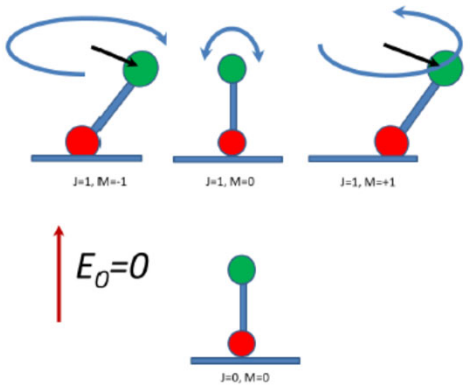

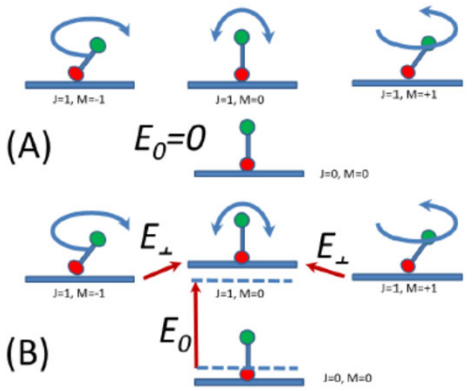

Goran Branković, and et al. New technique for gas sensing: Experiment results, University of Belgrade, Institute for Multidisciplinary Research, and Center for Nonlinear Sciences and Department of Physics, University of North Texas, USA (in progress);

Z Branković, Y Rostovtsev, A resonant single frequency molecular detector with high sensitivity and selectivity for gas mixtures, Scientific Reports 10, 1537 (2020)

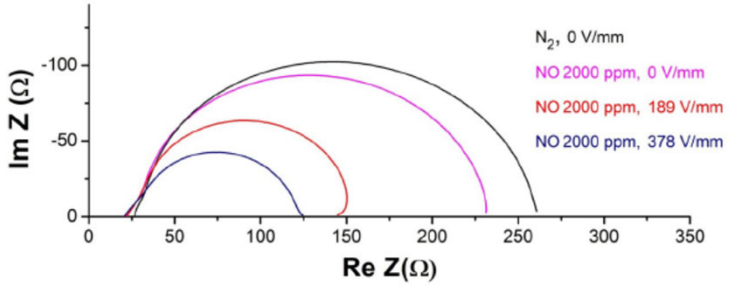

To build Maser (motivation)

Schawlow, A. L. & Townes, C. H. Infrared and optical masers. Phys. Rev. 112, 1940–1949 (1958).

Liang Jin1 , Matthias Pfender2, Nabeel Aslam2, Philipp Neumann2, Sen Yang2, Jo¨rg Wrachtrup2 & Ren-Bao Liu, Proposal for a room-temperature diamond maser, Nat. Commun. 6:8251 doi: 10.1038/ncomms9251 (2015).

Breeze, J., Salvadori, E., Sathian, J. *et al.* Continuous-wave room-temperature diamond maser. *Nature* **555,** 493–496 (2018). https://doi.org/10.1038/nature25970

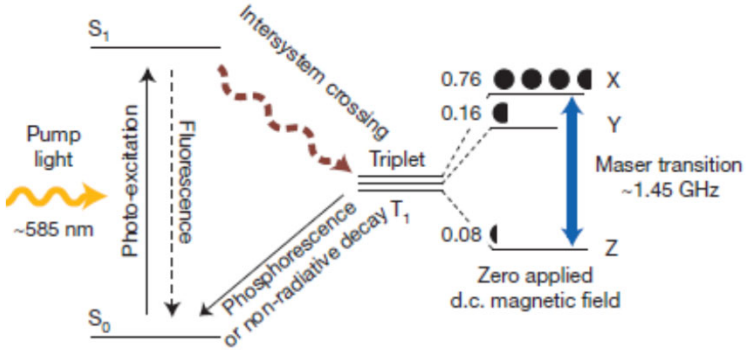

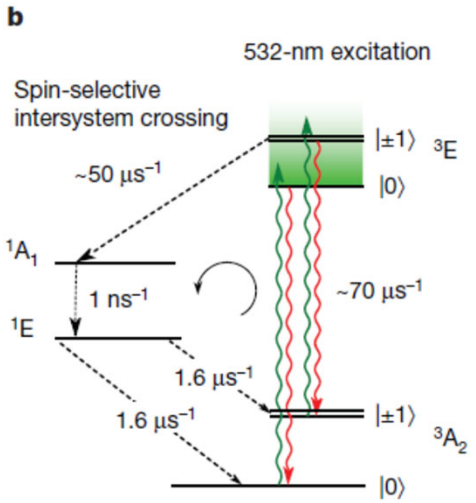

To build Maser

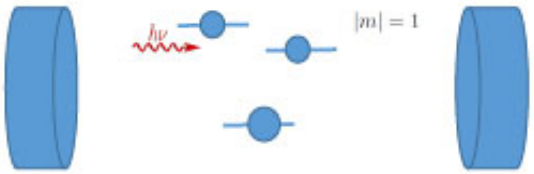

$$\dot{\Omega}_s = -i(\omega_0 - \omega_s)\Omega_s + i\Omega_a^2\rho_{ab}$$

$$\Omega_a^2 = \frac{2\pi\omega_0\wp^2 N}{\hbar}$$

$$i\hbar\dot{\rho} = [\hat{H}, \rho].$$

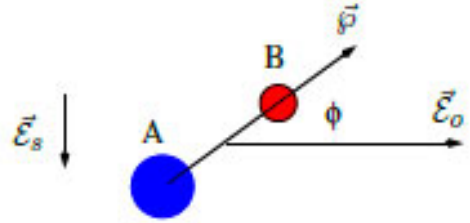

(a)

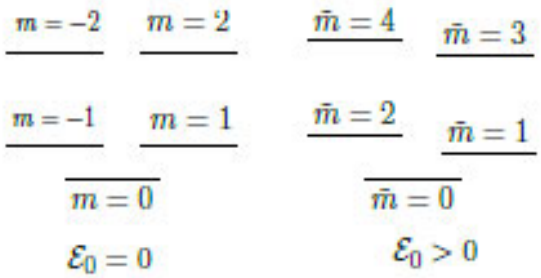

(b) (c)

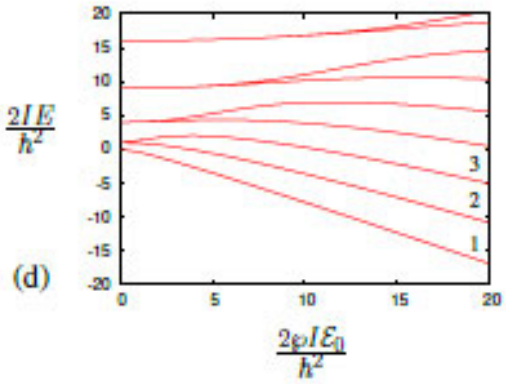

(d)

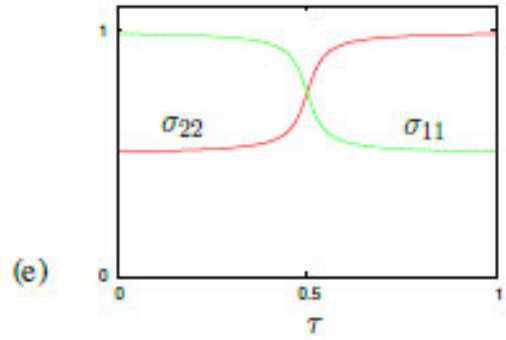

(e)

Maser pumping (at room temperature)

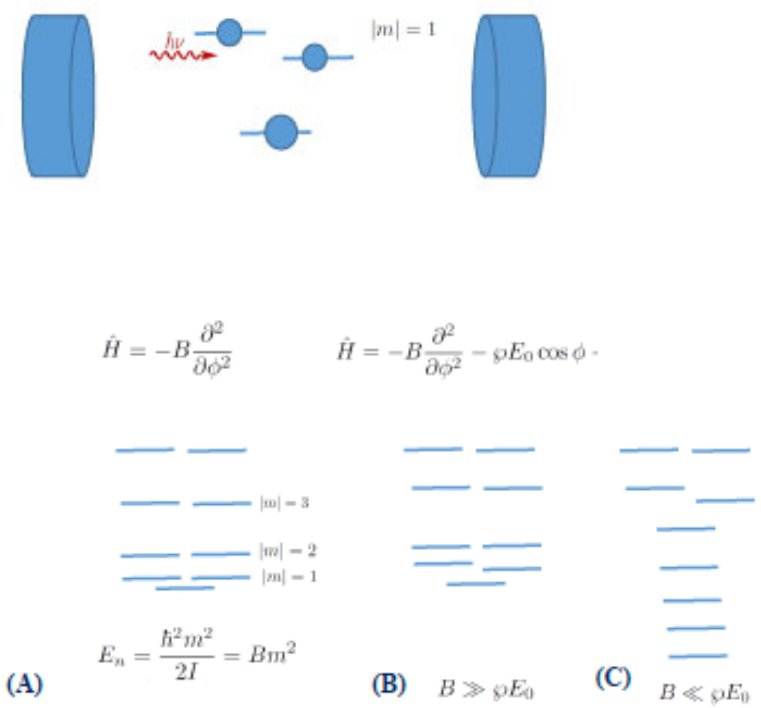

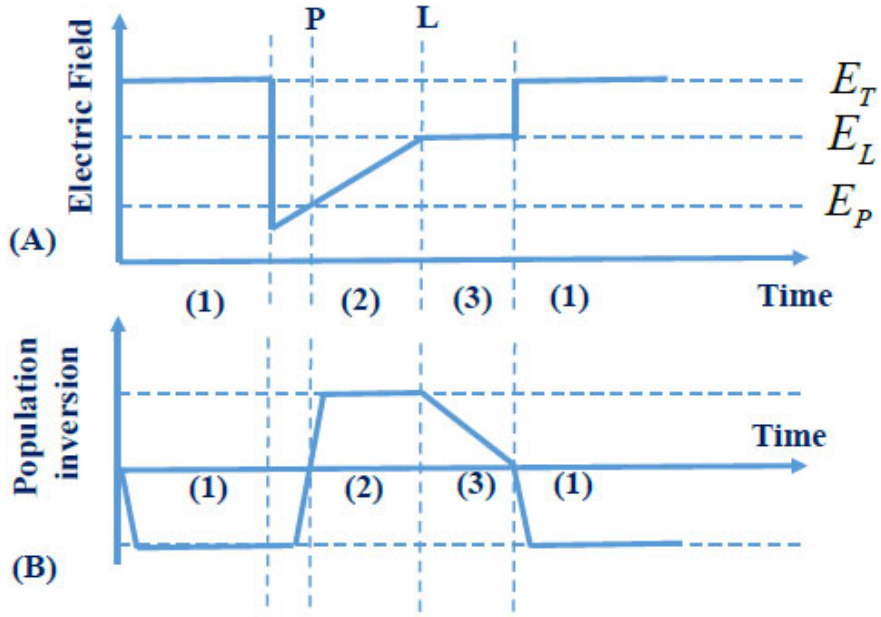

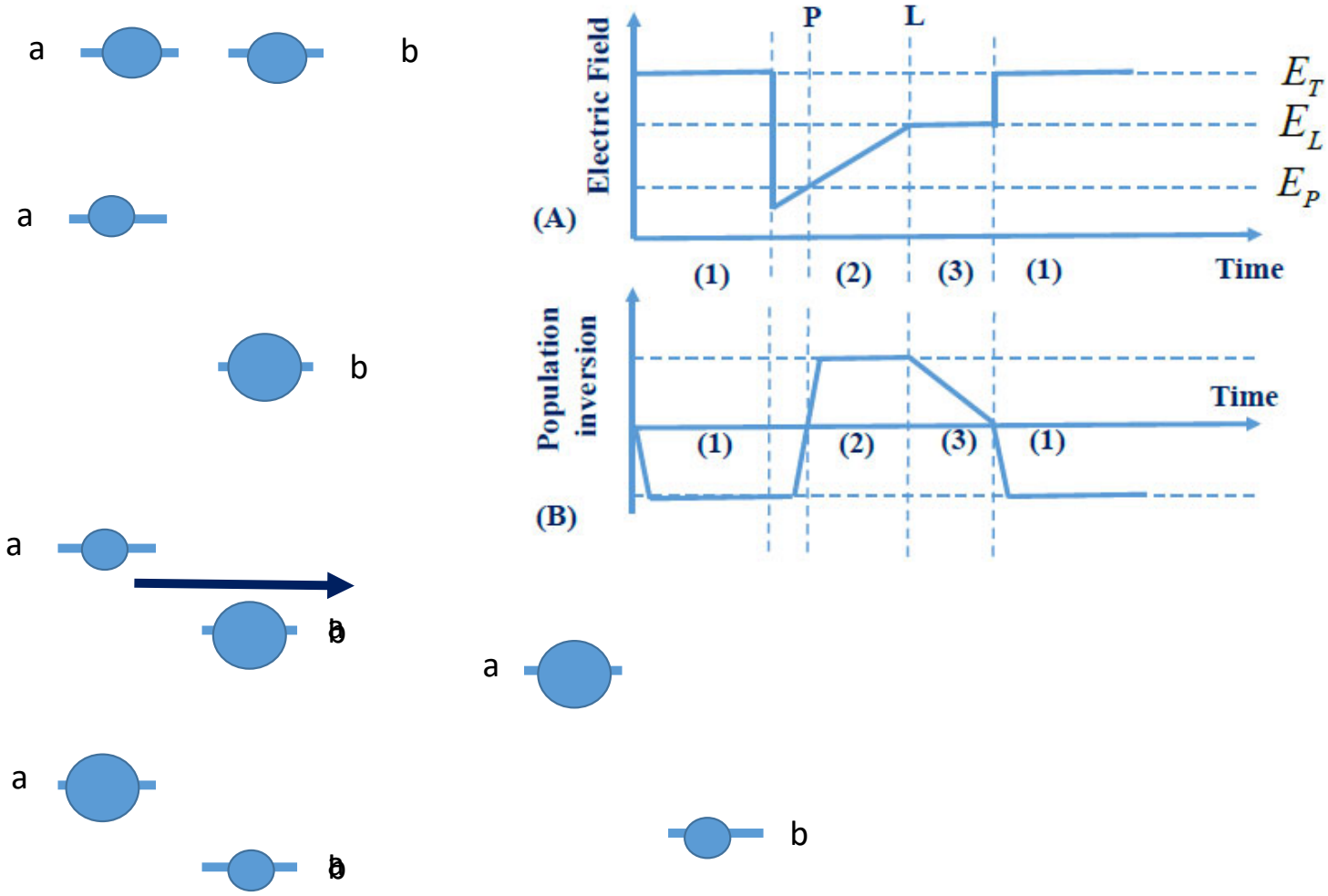
a
b
a
b
a
b
a
b
P
L
Electric Field
E_T
E_L
E_P
(A)
(1)
(2)
(3)
(1)
Time
Population inversion
Time
(1)
(2)
(3)
(1)
(B)

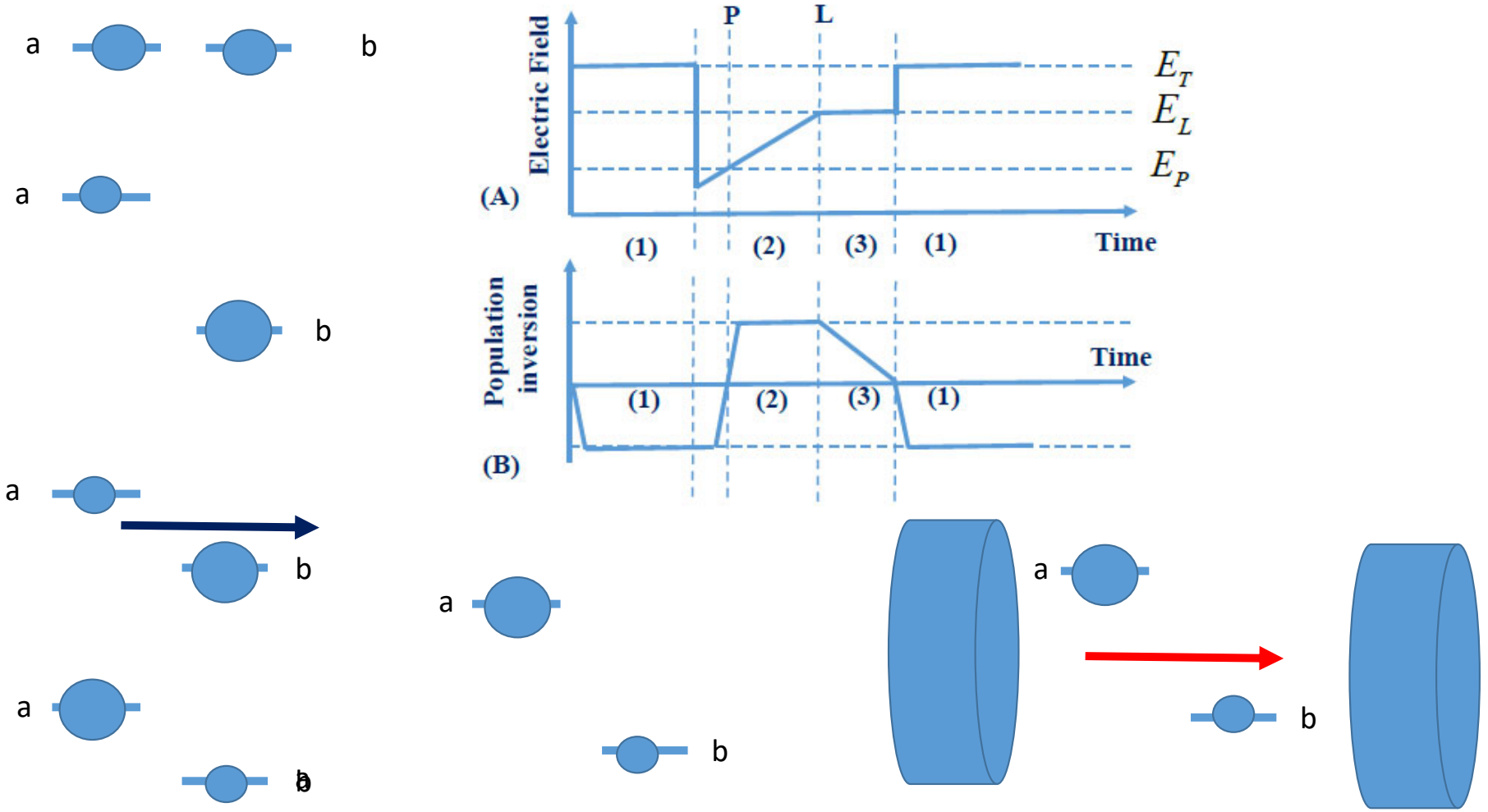
a
b
a
b
a
b
a
b
a
b
P
L
Electric Field
E_T
E_L
E_P
(A)
(1)
(2)
(3)
(1)
Time
Population inversion
Time
(1)
(2)
(3)
(1)
(B)

- Metropolitan networks via fiber
- Inter-city networks connected by quantum repeaters
- Long-distance quantum communication between satellite and ground

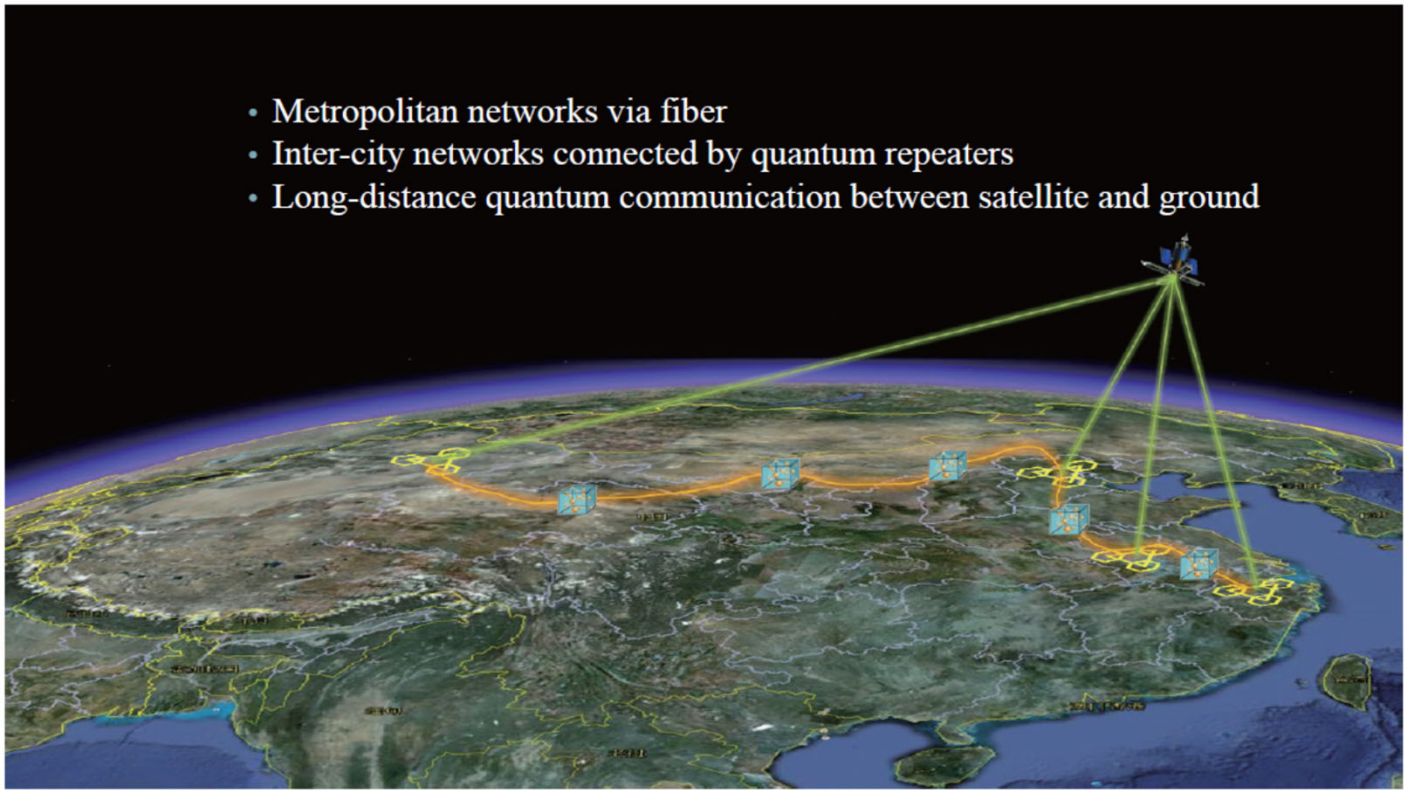

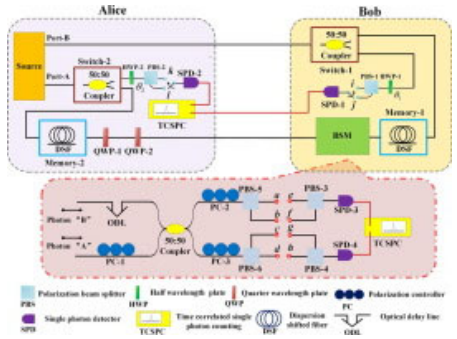

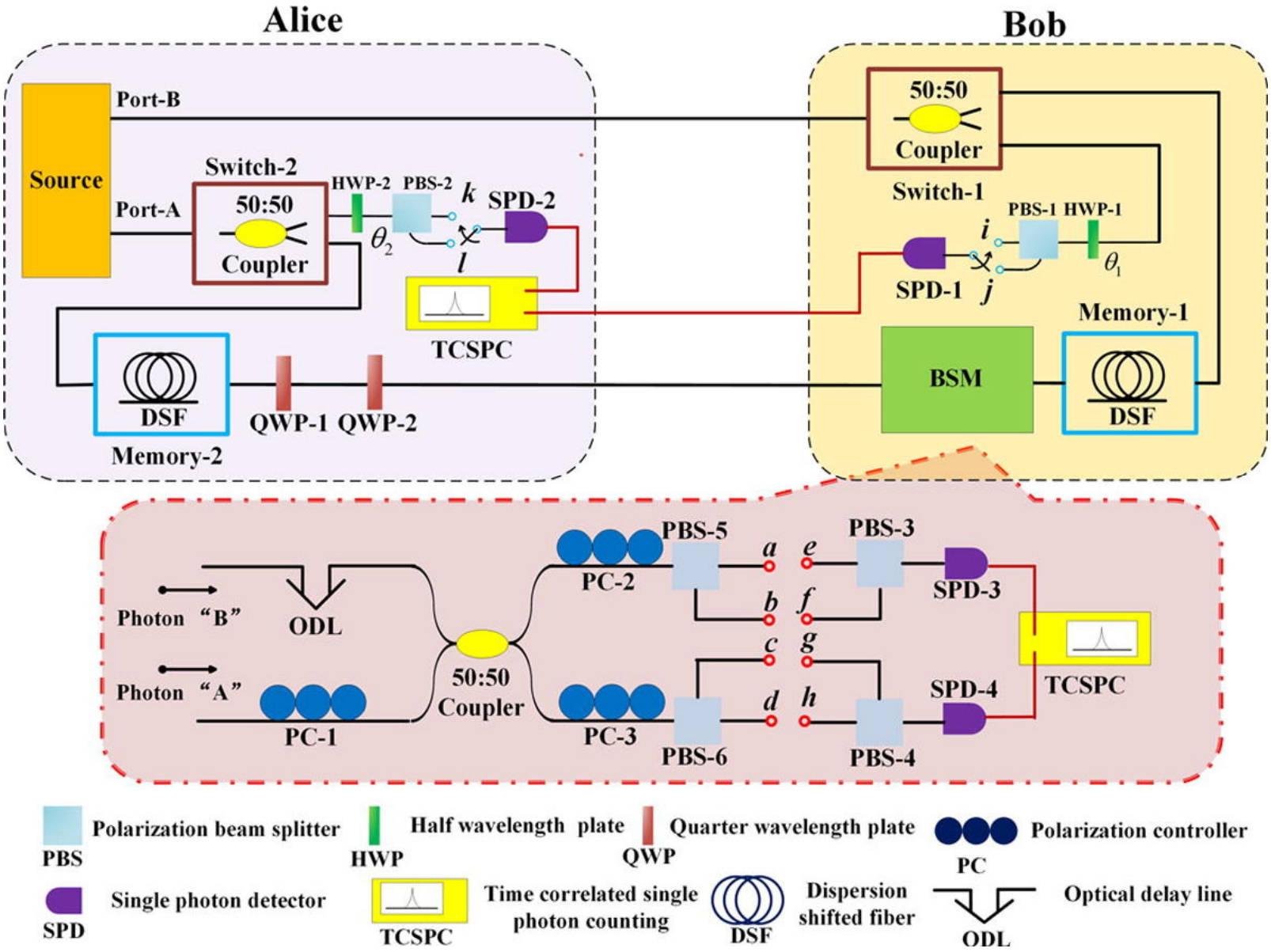
Alice
Bob
Source
Port-B
Port-A
Switch-2
50:50
Coupler
HWP-2
PBS-2
k
SPD-2
θ_2
l
TCSPC
DSF
Memory-2
QWP-1
QWP-2
50:50
Coupler
Switch-1
PBS-1
HWP-1
i
θ_1
SPD-1
j
Memory-1
BSM
DSF
Photon "B"
ODL
Photon "A"
PC-1
50:50
Coupler
PC-2
PC-3
PBS-5
PBS-6
a
b
c
d
e
f
g
h
PBS-3
PBS-4
SPD-3
SPD-4
TCSPC
Polarization beam splitter
PBS
Half wavelength plate
HWP
Quarter wavelength plate
QWP
Polarization controller
PC
Single photon detector
SPD
Time correlated single photon counting
TCSPC
Dispersion shifted fiber
DSF
Optical delay line
ODL

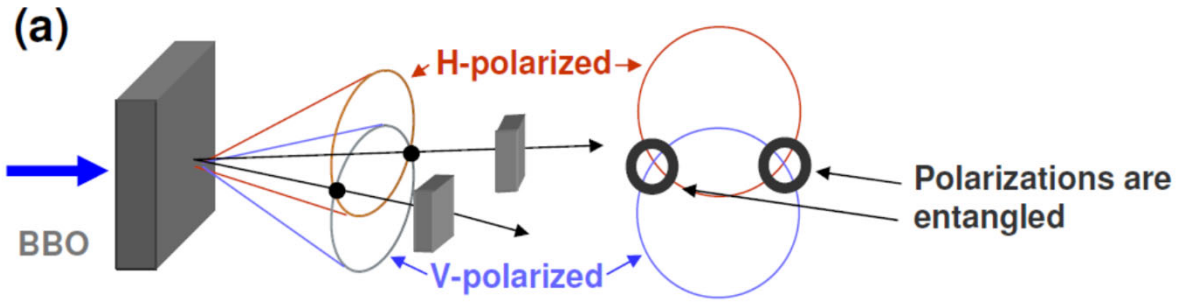

$$|\Psi\rangle = \frac{|1_V\rangle_1|1_H\rangle_2 + |1_H\rangle_1|1_V\rangle_2}{\sqrt{2}}$$

Barium borate (BBO)

$g \sim \chi 2$

$$V_I = \hbar g(\hat{a}_1^+ \hat{a}_2^+ \hat{b} + \hat{b}^+ \hat{a}_1 \hat{a}_2)$$

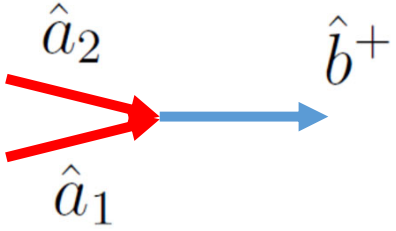

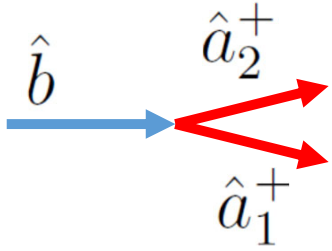

$$|\Psi\rangle = \sum_n B_{\beta,n}|\beta, n, n\rangle$$

$$|\Psi\rangle = \sum_n B_{n,\alpha}|n, \alpha, \alpha\rangle$$

$$B_{\beta,n} = (-ig\beta t)^n B_{\beta,0}$$

$$B_{n,\alpha} = \frac{(-ig\alpha^2 t)^n}{\sqrt{n!}} B_{0,\alpha}$$

$$|\Psi\rangle = (-ig\beta t)|1_1, 1_2\rangle + (-ig\beta t)^2|2_1, 2_2\rangle + \ldots$$

Quantum control and coherence in MoS_2 (2D) materials

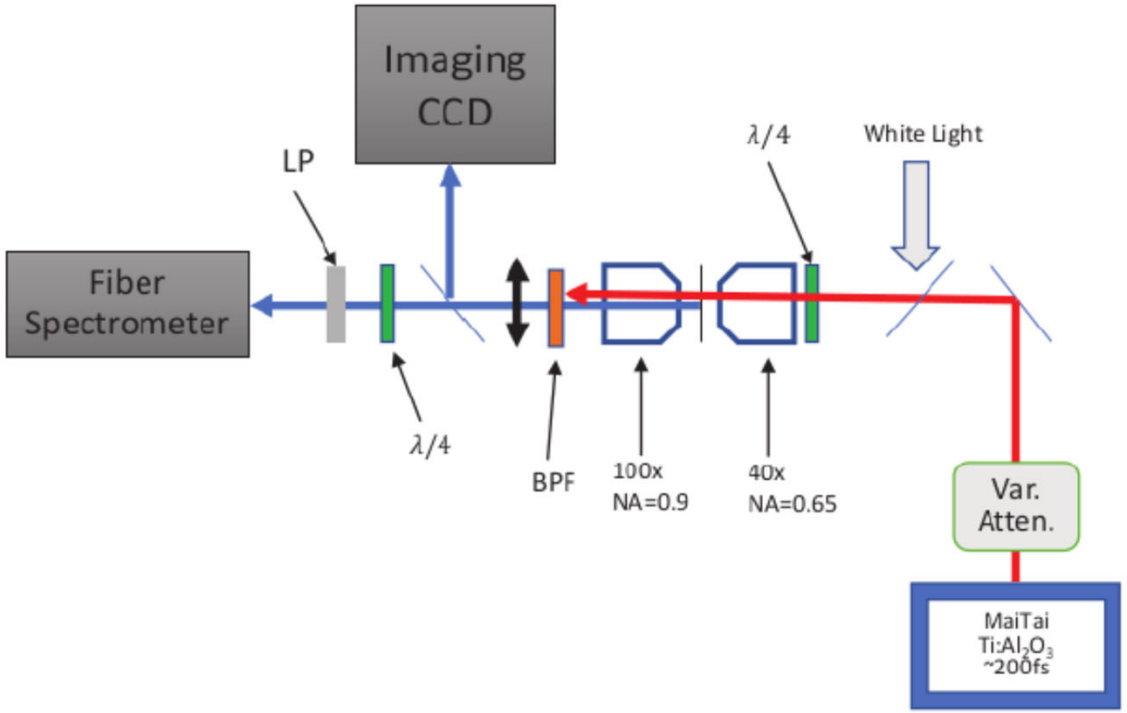

Figure 1: The experimental setup is shown.

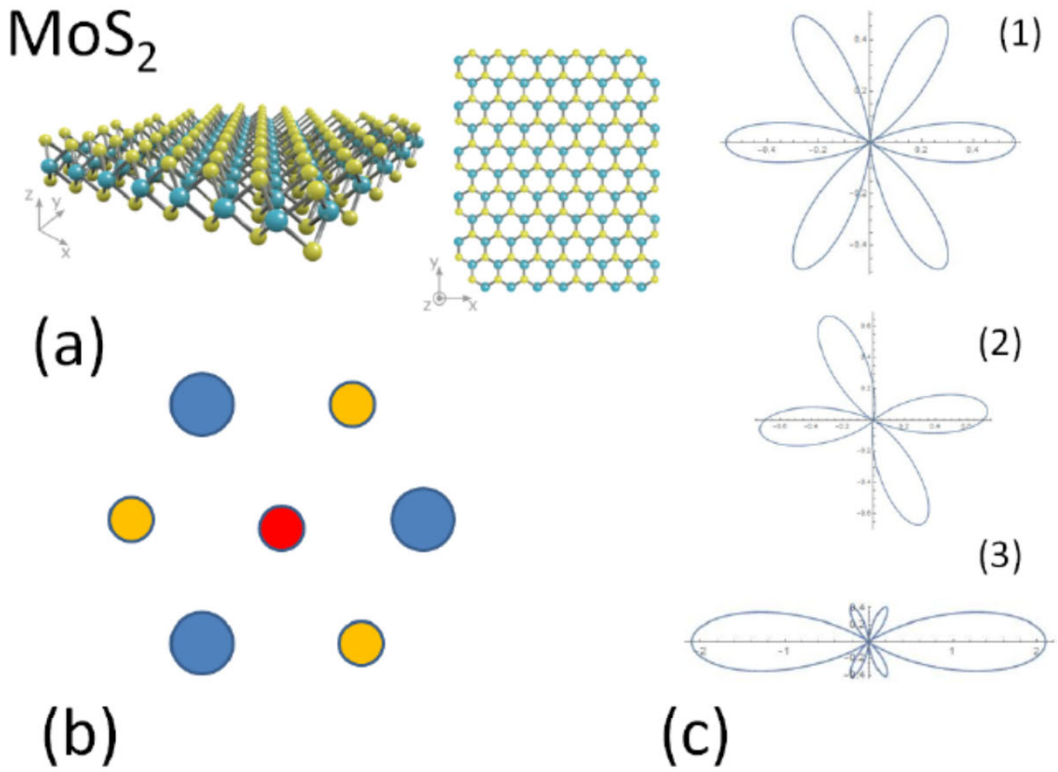

Figure 4: (a) MoS2 structure (b) Simplified view of just one lattice site (blue circles) and an exciton (red circle). (c) The polarization dependence with respect to the orientation of the laser field. (1) response of lattice, exciton response is much smaller; (2) lattice and exciton responses are comparable and (3) the exciton responce is much larger than lattice.

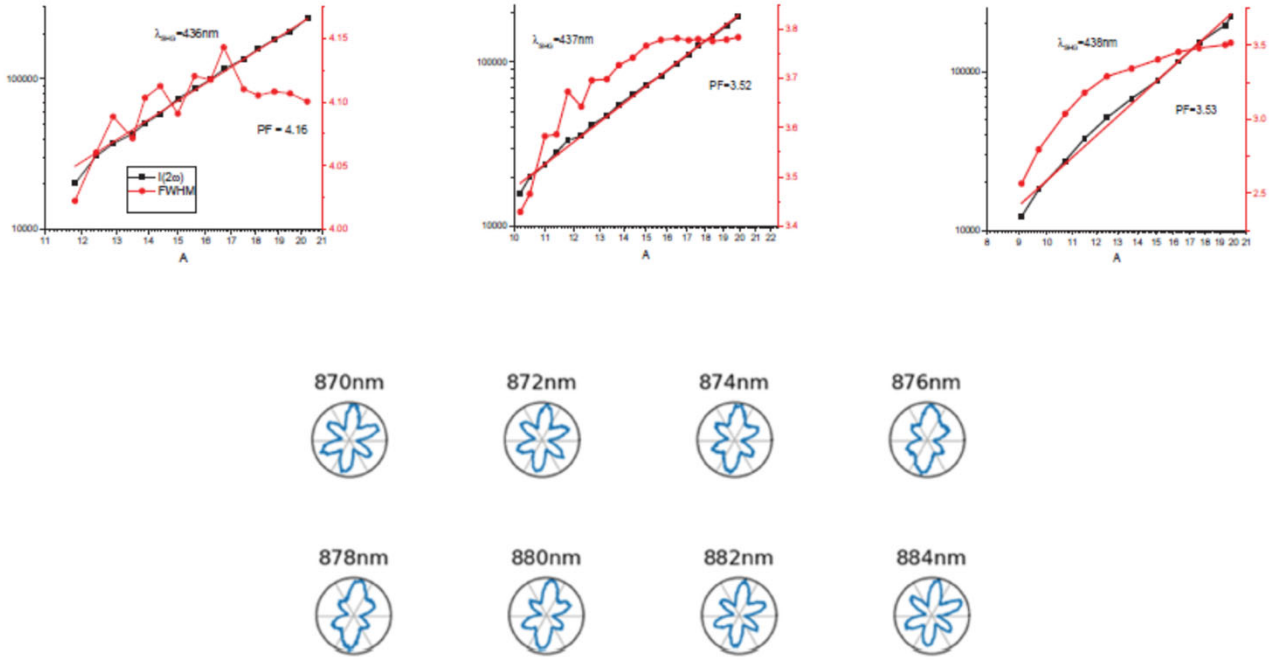

Figure 2: The dependence of the SHG signal and its width on the power of the pump laser for different wavelengths of the pump laser (upper panel). The polarization dependence of the SHG signal on the polarization of the pump laser for different wavelengths of the pump laser (lower panel).

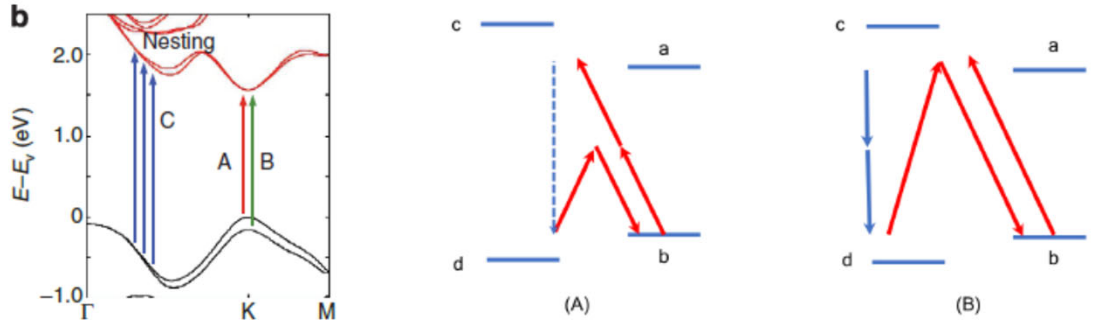

Figure 3: The inset represents the schematics of the density matrix model. We assume a is electronic excited state, and c_A and c_B represent the ground states that correspond to transitions $|a\rangle \rightarrow |c_A\rangle$ and $|a\rangle \rightarrow |c_B\rangle$ related to A-exciton and B-exciton correspondingly. We show also the states b_A and b_B representing the vibrational states related to the phonon excitaion in the syste. The energy of vibrtaion is 40 meV that is lager than the energy corresponds to the termal energy at the room temperature 25 meV, we assume that initially the vibrational states are empty. We show the pump and delayed probe fields.

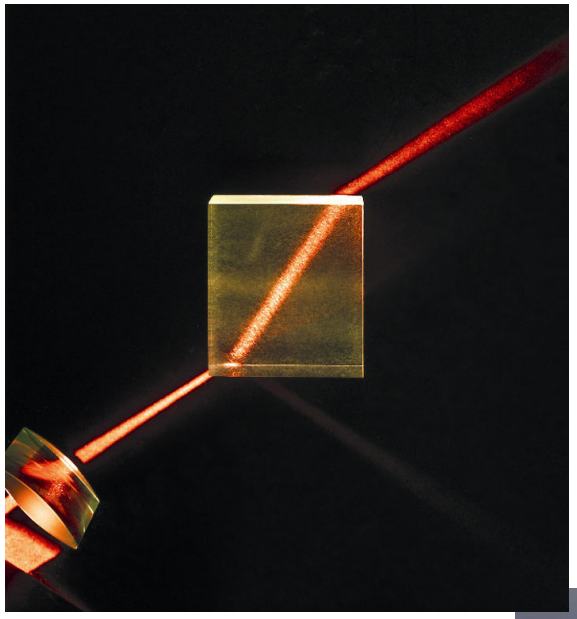

Angular dispersion

Prisms:

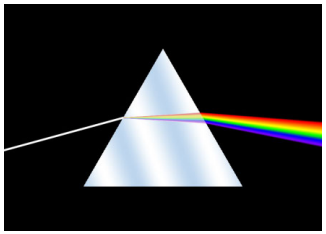

$$d\theta/d\lambda = 10^{-4}\ \mathrm{nm}^{-1}$$

Diffraction gratings
Interferometers

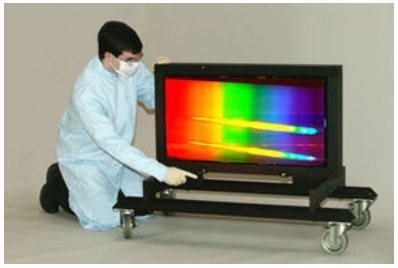

$$d\theta/d\lambda = 10^{-3}\ \mathrm{nm}^{-1}$$

What is angular dispersion of media with excited quantum coherence?

Angular dispersion

Prisms:

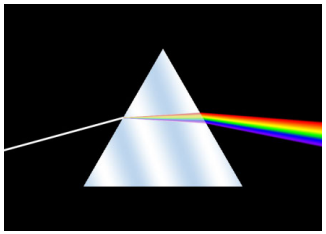

$$d\theta/d\lambda = 10^{-4}\ \mathrm{nm}^{-1}$$

Diffraction gratings
Interferometers

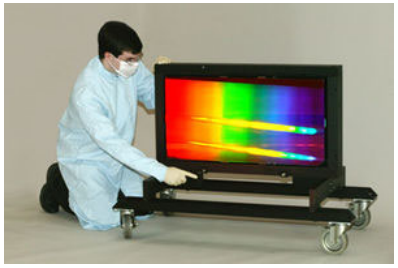

$$d\theta/d\lambda = 10^{-3}\ \mathrm{nm}^{-1}$$

The medium with excited quantum coherence

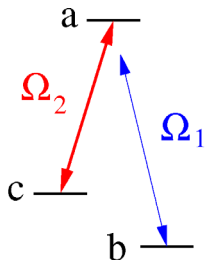

$$d\theta/d\lambda = 10^{3}\ \mathrm{nm}^{-1}$$

V.A. Sautenkov, *et al.,* Ultra-dispersive adaptive prism, Phys. Phys. Rev. A **81**, 063824 (2010), quant-ph/0701229

Quantum fields

$$|\psi\rangle = \sum_k \alpha_k |1_k\rangle$$

$$\hat{E} = \sum_k (\hat{a}_k \exp[ikz - i\omega t] + \hat{a}_k^+ \exp[-ikz + i\omega t]) = \hat{E}^{(+)} + \hat{E}^{(-)}$$

$$\langle E^2 \rangle = \langle \psi | \hat{E}^{(-)} \hat{E}^{(+)} | \psi \rangle = \langle \psi | \hat{E}^{(-)} \left(\sum_n |n\rangle\langle n| \right) \hat{E}^{(+)} | \psi \rangle = \left| \langle 0 | \hat{E}^{(+)} | \psi \rangle \right|^2$$

$$\alpha_k = \exp[-\frac{k^2 L^2}{2}]$$

$$\langle E^2 \rangle = \left| \langle 0 | \hat{E}^{(+)} | \psi \rangle \right|^2 = \exp\left[-\frac{(z - ct)^2}{L^2} \right]$$

One Mode of the Quantum field

$$v(z,t) = \sum \alpha_k e^{ikz - i\omega_k t} = \exp\left[ik_0 z - i\omega_0 t - \frac{(z-ct)^2}{2L^2}\right]$$

$$\hat{E} = E_0(v(z,t)\hat{b} + v(z,t)^*\hat{b}^+) = \hat{E}^{(+)} + \hat{E}^{(-)}$$

$$E_0 = \sqrt{2\pi\hbar\omega_0/V}$$

A two-level atom

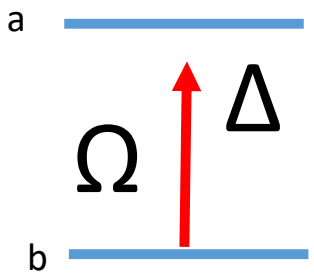

$\omega_{ab} = (E_a - E_b)/\hbar$ is

$$\hat{V}_I = -\hat{\wp} \cdot \hat{E} = \wp_{ab} E_0 \left(v(z,t) e^{i\omega_{ab}t} |a\rangle\langle b| \hat{b} + \hat{b}^{+} v^{*}(z,t) e^{-i\omega_{ab}t} |b\rangle\langle a| \right)$$

A two-level atom interacting with quantum field

$$|\Psi\rangle = A|a,0\rangle + B|b,1\rangle$$

$$i\hbar\frac{\partial}{\partial t}|\Psi\rangle = \hat{V}_I|\Psi\rangle$$

$$\dot{A} = -i\Omega_0 e^{ik_0 z + i\delta_0 t} V B$$
$$\dot{B} = -i\Omega_0 e^{-ik_0 z - i\delta_0 t} V^* A$$

A two-level atom interacting with quantum field

$$\mathcal{E} = \langle 0|\hat{E}^{(+)}|\Psi\rangle \simeq$$

$$E_0 \exp\left[ik_0 z - i\left(\omega_0 + \frac{\Omega_0^2}{\delta_0}|V|^2\right)t\right] B_0 V\left[z - \left(c + c\frac{\Omega_0^2}{\delta_0^2}|V|^2\right)t\right]$$

$$V_{ph} = \frac{\omega_0 + \dfrac{\Omega_0^2|V|^2}{\delta_0}}{k} \qquad V_g = \frac{\partial}{\partial k}\left(\omega_0 + \frac{\Omega_0^2|V|^2}{\delta_0}\right) = c + c\frac{\Omega_0^2}{\delta_0^2}|V|^2$$

Mach-Zehnder interferometer

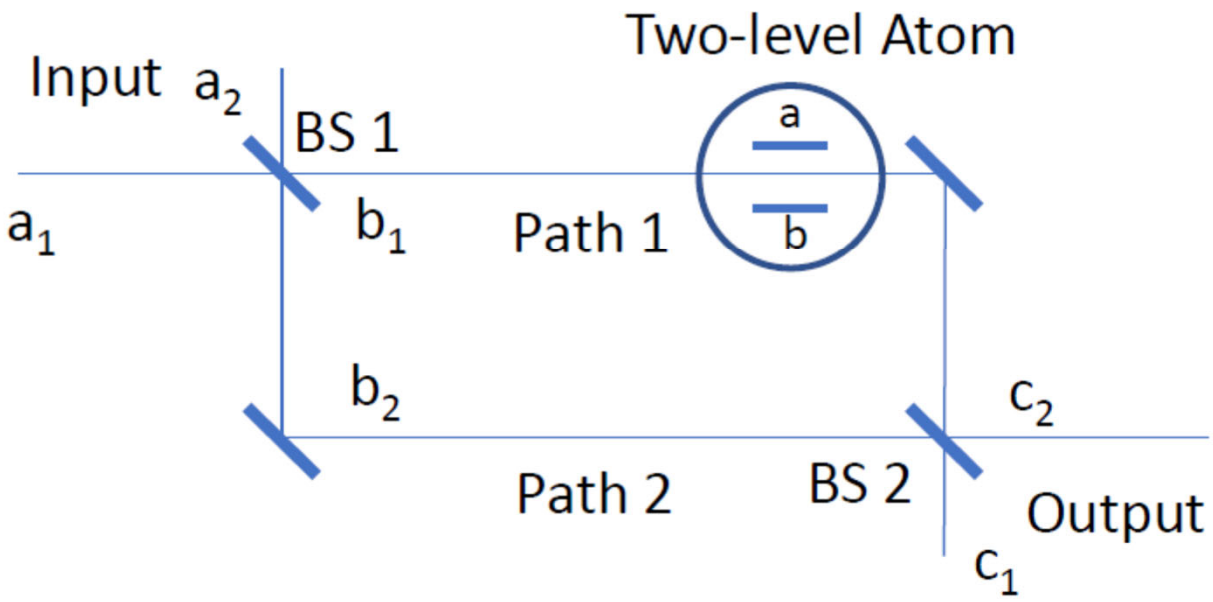

Mach-Zehnder interferometer

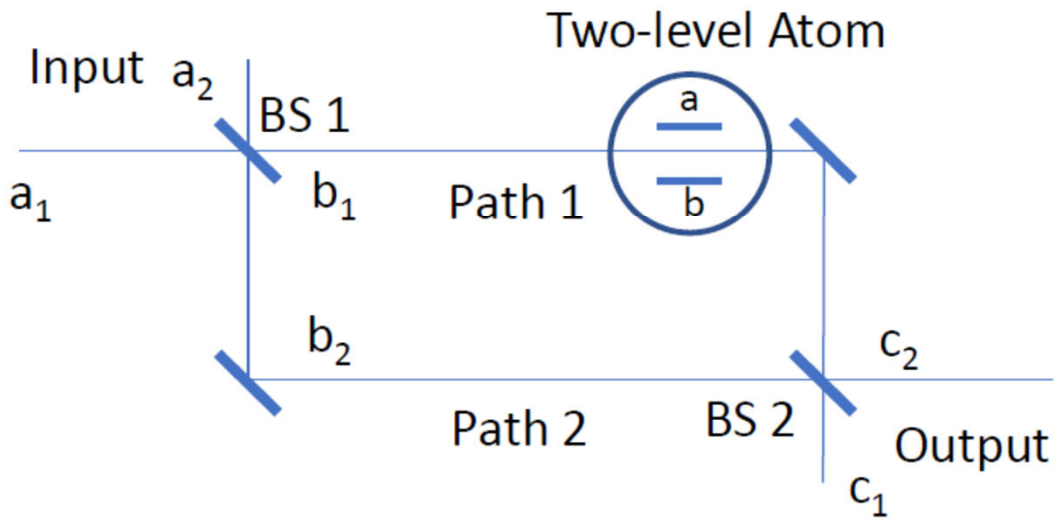

$$\begin{pmatrix} \hat{b}_1 \\ \hat{b}_2 \end{pmatrix} = \begin{pmatrix} \cos\zeta & -i\sin\zeta \\ -i\sin\zeta & \cos\zeta \end{pmatrix} \begin{pmatrix} \hat{a}_1 \\ \hat{a}_2 \end{pmatrix} = S \begin{pmatrix} \hat{a}_1 \\ \hat{a}_2 \end{pmatrix} S^{+}$$

$$S = \exp\left[i\zeta\left(\hat{a}_1^{+}\hat{a}_2 + \hat{a}_1\hat{a}_2^{+}\right)\right],$$

$$\begin{pmatrix} \hat{b}_1 \\ \hat{b}_2 \end{pmatrix} == S_1 \begin{pmatrix} \hat{a}_1 \\ \hat{a}_2 \end{pmatrix} S_1^{+}$$

$$\begin{pmatrix} \hat{c}_1 \\ \hat{c}_2 \end{pmatrix} = S_2 \begin{pmatrix} \hat{b}_1 \\ \hat{b}_2 \end{pmatrix} S_2^{+}$$

Mach-Zehnder interferometer

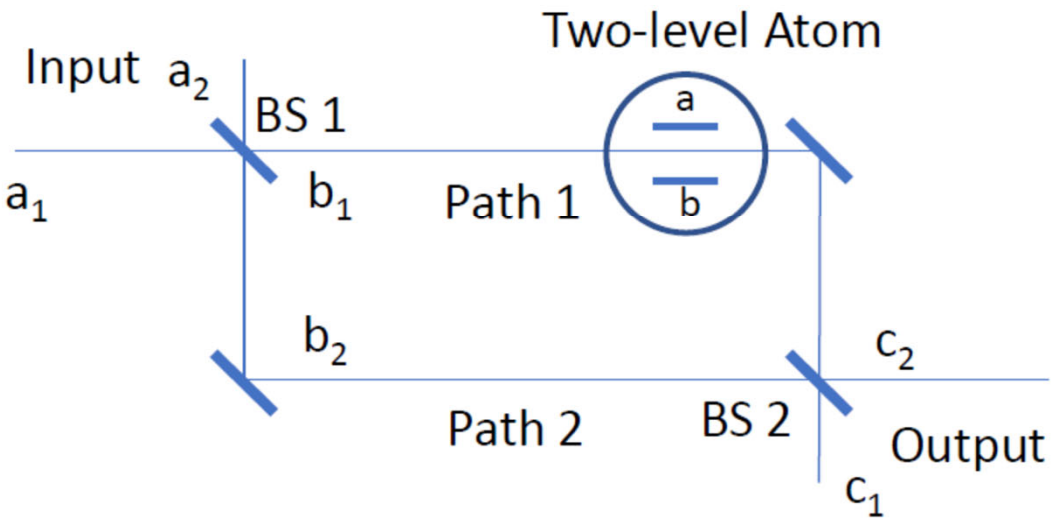

$$\begin{pmatrix} \hat{b}_1 \\ \hat{b}_2 \end{pmatrix} == S_1 \begin{pmatrix} \hat{a}_1 \\ \hat{a}_2 \end{pmatrix} S_1^+$$

$$\begin{pmatrix} \hat{c}_1 \\ \hat{c}_2 \end{pmatrix} = S_2 \begin{pmatrix} \hat{b}_1 \\ \hat{b}_2 \end{pmatrix} S_2^+$$

Mach-Zehnder interferometer

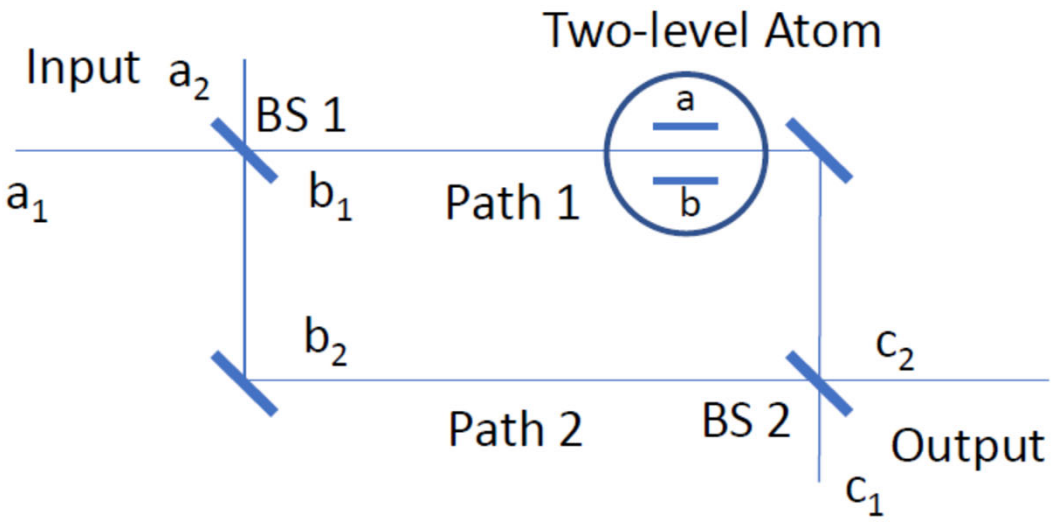

$$\begin{pmatrix} \hat{b}_1 \\ \hat{b}_2 \end{pmatrix} \rightarrow \begin{pmatrix} 1 & 0 \\ 0 & \exp[i\phi] \end{pmatrix} \begin{pmatrix} \hat{b}_1 \\ \hat{b}_2 \end{pmatrix} = U \begin{pmatrix} \hat{b}_1 \\ \hat{b}_2 \end{pmatrix} U^+$$

$$|\text{out}\rangle = MZ|1,0\rangle = S_2 U S_1 |1,0\rangle = \frac{e^{i\phi}-1}{2}|1,0\rangle + \frac{e^{i\phi}+1}{2}|0,1\rangle$$

Mach-Zehnder interferometer

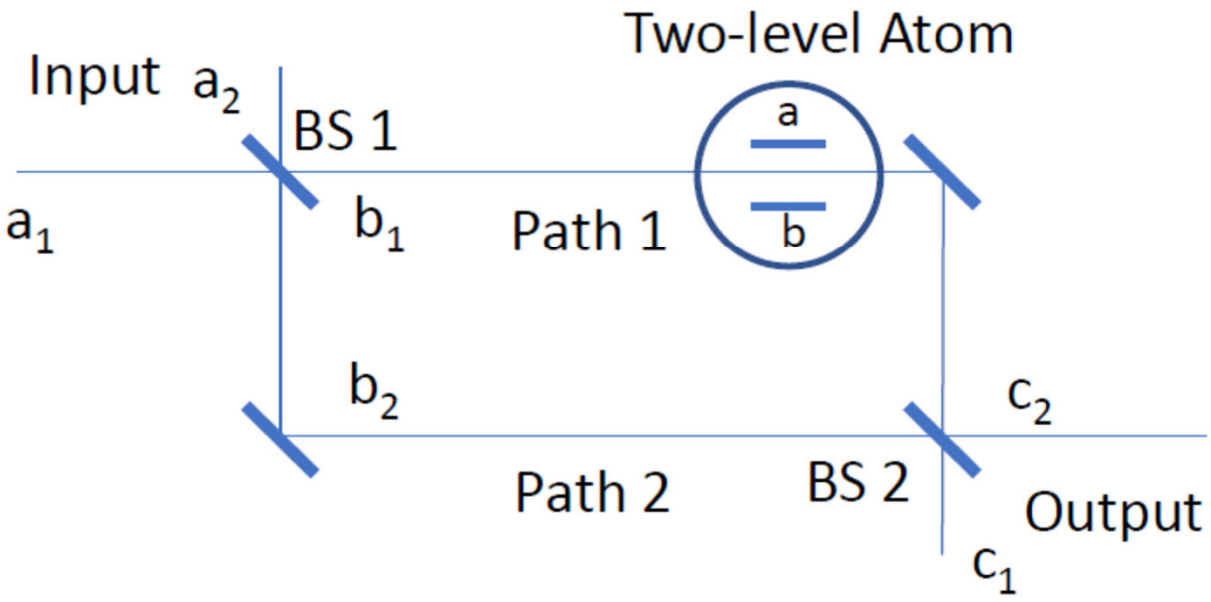

$$\hat{E}(z,t) = E_0 \begin{cases} v_{1a}\hat{a}_1 + v_{1a}^*\hat{a}_1^+ & z_1 < z_{BS_1} \\ v_{2a}\hat{a}_2 + v_{2a}^*\hat{a}_2^+ & z_2 < z_{BS_1} \\ v_{1b}\hat{b}_1 + v_{1b}^*\hat{b}_1^+ & z_{BS_1} < z_1 < z_{BS_2} \\ v_{2b}\hat{b}_2 + v_{2b}^*\hat{b}_2^+ & z_{BS_1} < z_2 < z_{BS_2} \\ v_{1c}\hat{c}_1 + v_{1c}^*\hat{c}_1^+ & z_1 > z_{BS_2} \\ v_{1c}\hat{c}_2 + v_{2c}^*\hat{c}_2^+ & z_2 > z_{BS_2} \end{cases}$$

$$v_{1,2a}(z_{1,2},t) = \exp\left[ik_0 z_{1,2} - i\omega_0 t - \frac{(z_{1,2}-ct)^2}{2L^2}\right]$$

$$v_{1,2b}(z_{1,2},t) = \exp\left[ik_0 z_{1,2} - i\omega_0 t - \frac{(z_{1,2}-ct)^2}{2L^2}\right]$$

$$v_{1,2c}(z_{1,2},t) = \exp\left[ik_0 z_{1,2} - i\omega_0 t - \frac{(z_{1,2}-ct)^2}{2L^2}\right].$$

$$\frac{B-B_0}{2} = \frac{e^{i\phi_A}-1}{2}B_0 \simeq i\frac{\phi_A}{2}$$

$$\hat{E} = E_0(v(z,t)\hat{b} + v(z,t)^*\hat{b}^+) = \hat{E}^{(+)} + \hat{E}^{(-)}$$

$$|\Psi\rangle = \hat{T}\exp\left[-\frac{i}{\hbar}\int_0^t dt' V_I(t')\right]|\Psi_0\rangle \simeq \exp[-i\phi_A]|\Psi_0\rangle,$$

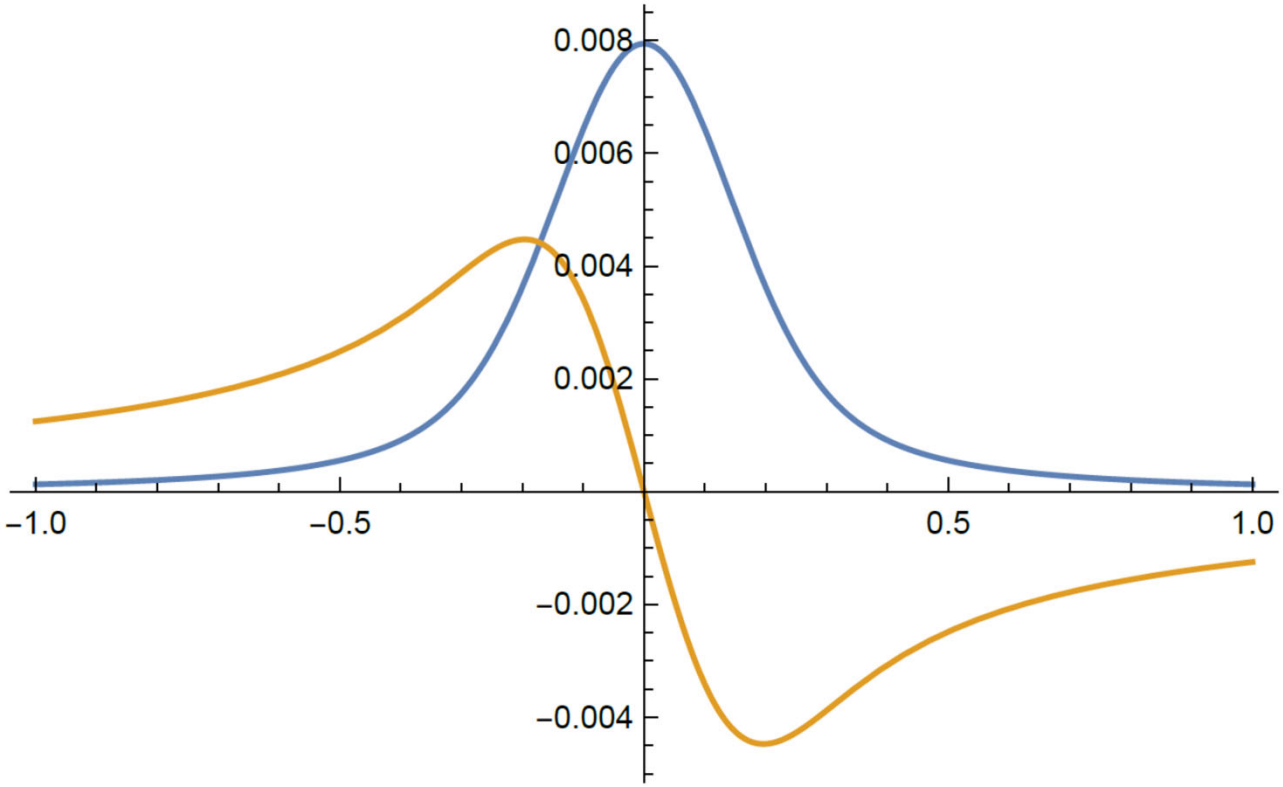

Figure 3. Mach-Zehnder interferometer signal imaginary and real parts.

$$|\Psi\rangle = B_0|B,1_0\rangle + \sum_{k_\perp} B_\perp|B,1_\perp\rangle + \sum_j A_j|a_j,0\rangle$$

$$|B,1_0\rangle = |b_1 b_2 ... b_{\mathcal{N}},1_0\rangle,\ |a_j,0\rangle = |b_1 b_2 ... a_j ... b_{\mathcal{N}},0\rangle$$

$$\hat{E} = E_0(v_0(r,t)\hat{b}_0 + v_0(r,t)^*\hat{b}_0^+) + \sum_{k_\perp} E_{k_\perp}(v_{k_\perp}(z,t)\hat{b}_{k_\perp} + v_{k_\perp}(z,t)^*\hat{b}_{k_\perp}^+)$$

$$v(r,t) = e^{ik_0 r - i\omega_0 t}\tilde{V}_0(r,t)$$

$$v_{k_\perp}(r,t) = e^{ik_\perp r - i\omega_0 t}\tilde{V}_{k_\perp}(r,t)$$

$$E_0 = \sqrt{2\pi\hbar\omega_0/V},\ E_{k_\perp} = \sqrt{2\pi\hbar\omega_{k_\perp}/V}$$

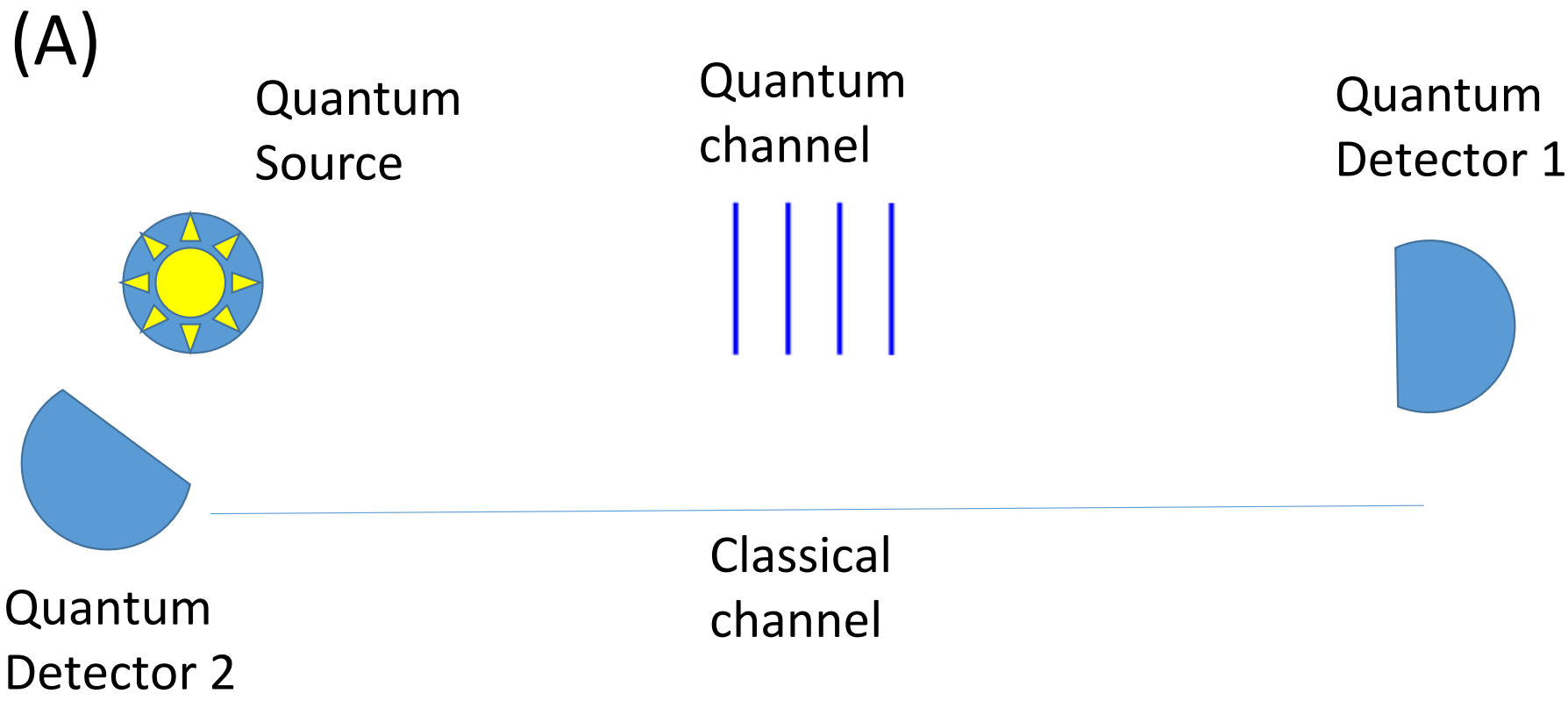
(A)
Quantum Source
Quantum channel
Quantum Detector 1
Quantum Detector 2
Classical channel

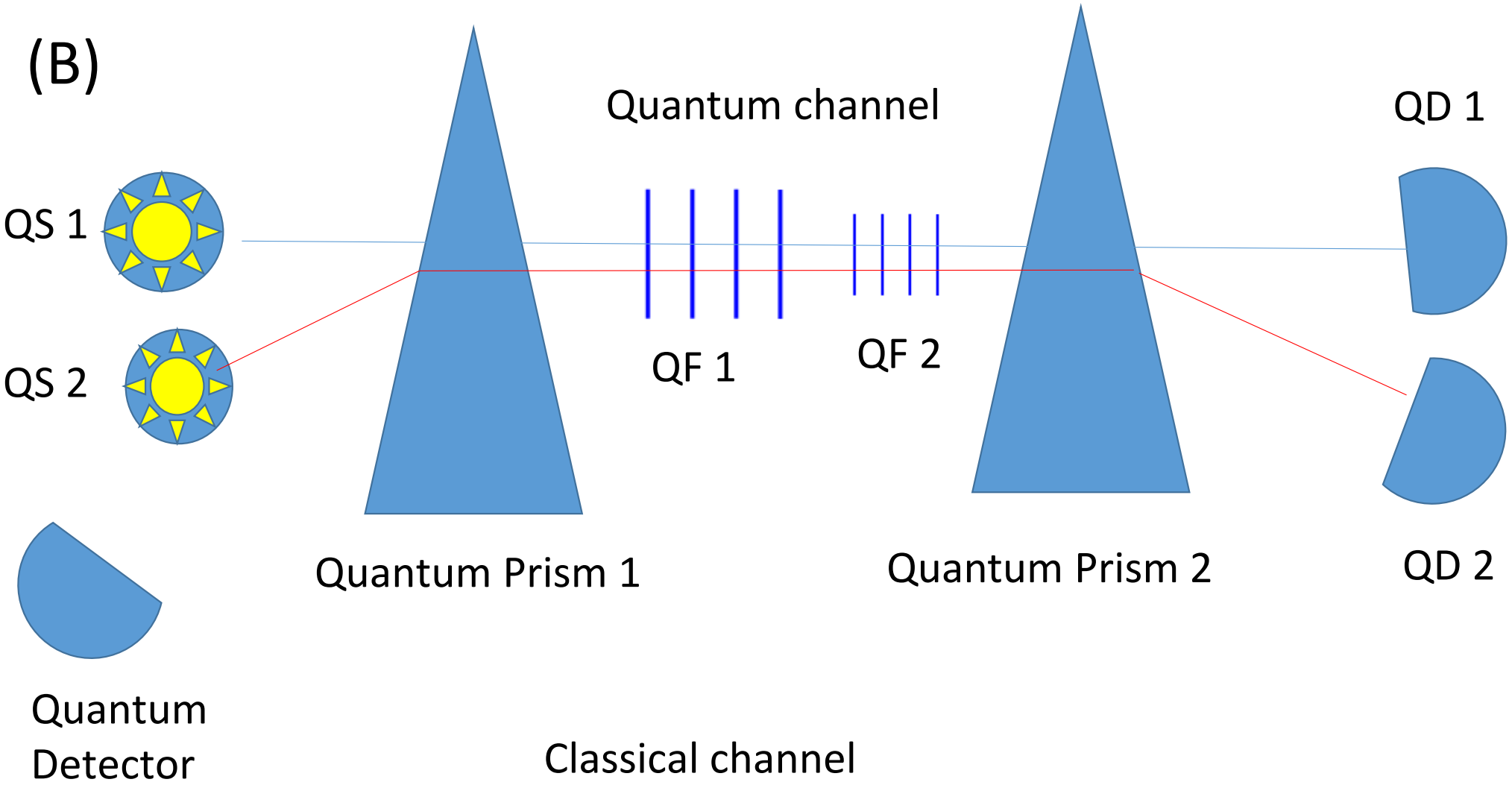
(B)
Quantum channel
QD 1
QS 1
QS 2
QF 1
QF 2
Quantum Prism 1
Quantum Prism 2
QD 2
Quantum
Detector
Classical channel

CHIRAP in a two-level atomic system

$$\hat{H} = \hbar\Delta|a\rangle\langle a| + \hbar\Omega(|a\rangle\langle b| + |b\rangle\langle a|)$$

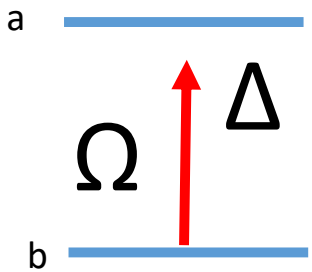

$$\lambda_{\pm} = \omega_{\pm} = \frac{\Delta}{2} \pm \sqrt{\left(\frac{\Delta}{2}\right)^2 + \Omega^2}$$

$$\omega_+(\Delta) = \begin{cases} 0, & \Delta \to -\infty \\ \Delta, & \Delta \to +\infty \end{cases} \quad \text{and} \quad |+\rangle(\Delta) = \begin{cases} |b\rangle, & \Delta \to -\infty \\ |a\rangle, & \Delta \to +\infty \end{cases}$$

$$\omega_-(\Delta) = \begin{cases} \Delta, & \Delta \to -\infty \\ 0, & \Delta \to +\infty \end{cases} \quad \text{and} \quad |-\rangle(\Delta) = \begin{cases} |a\rangle, & \Delta \to -\infty \\ |b\rangle, & \Delta \to +\infty \end{cases}$$

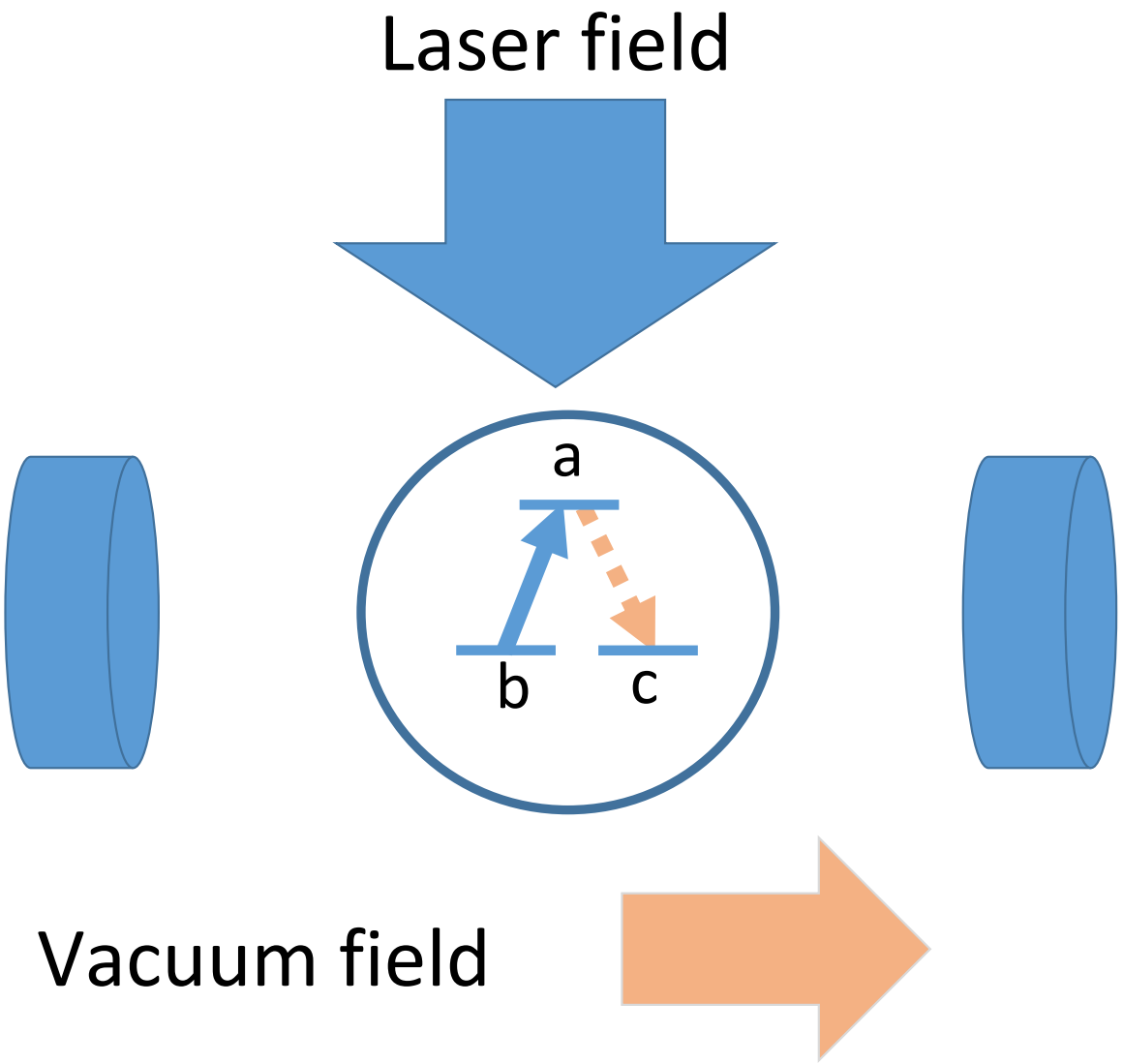

Colin Roy, et al., (2022).

Laser field

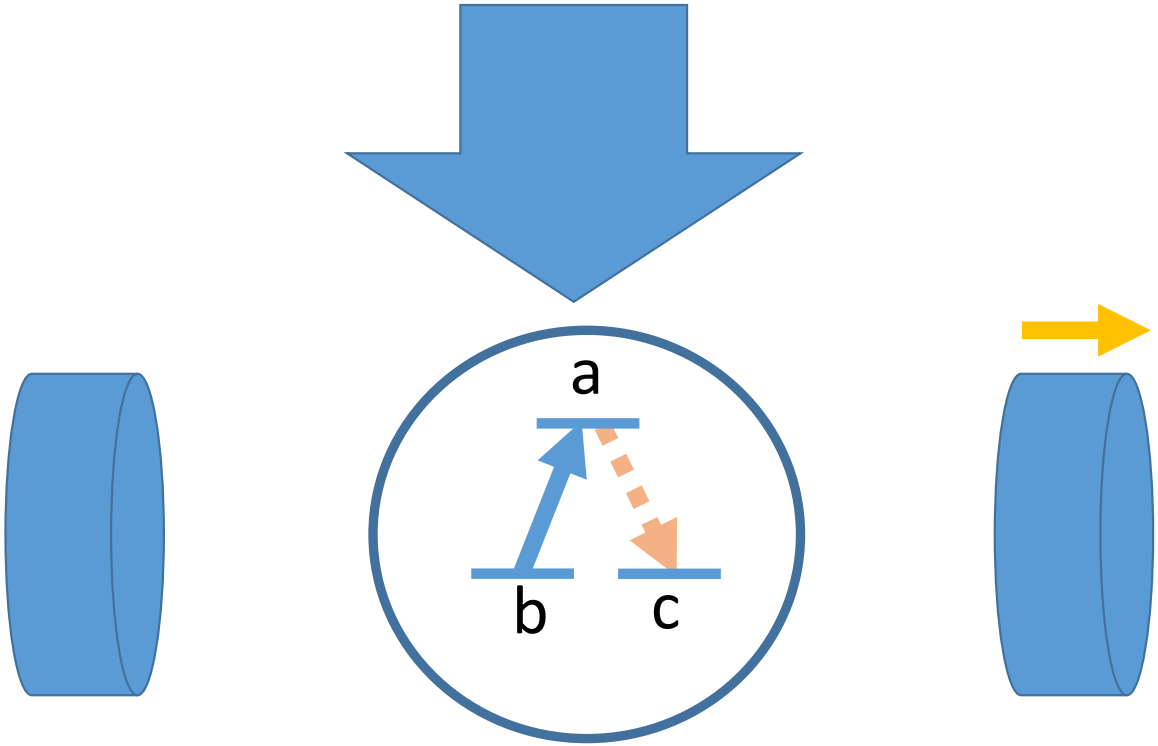

Vacuum field

Laser and vacuum Fields

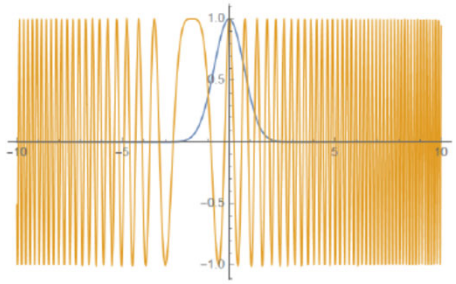

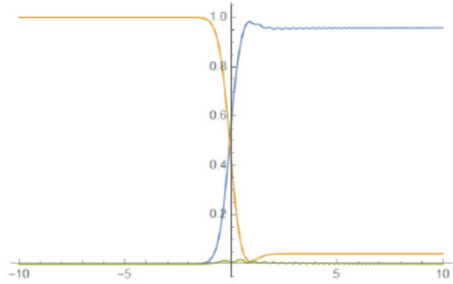

Populations in b and c

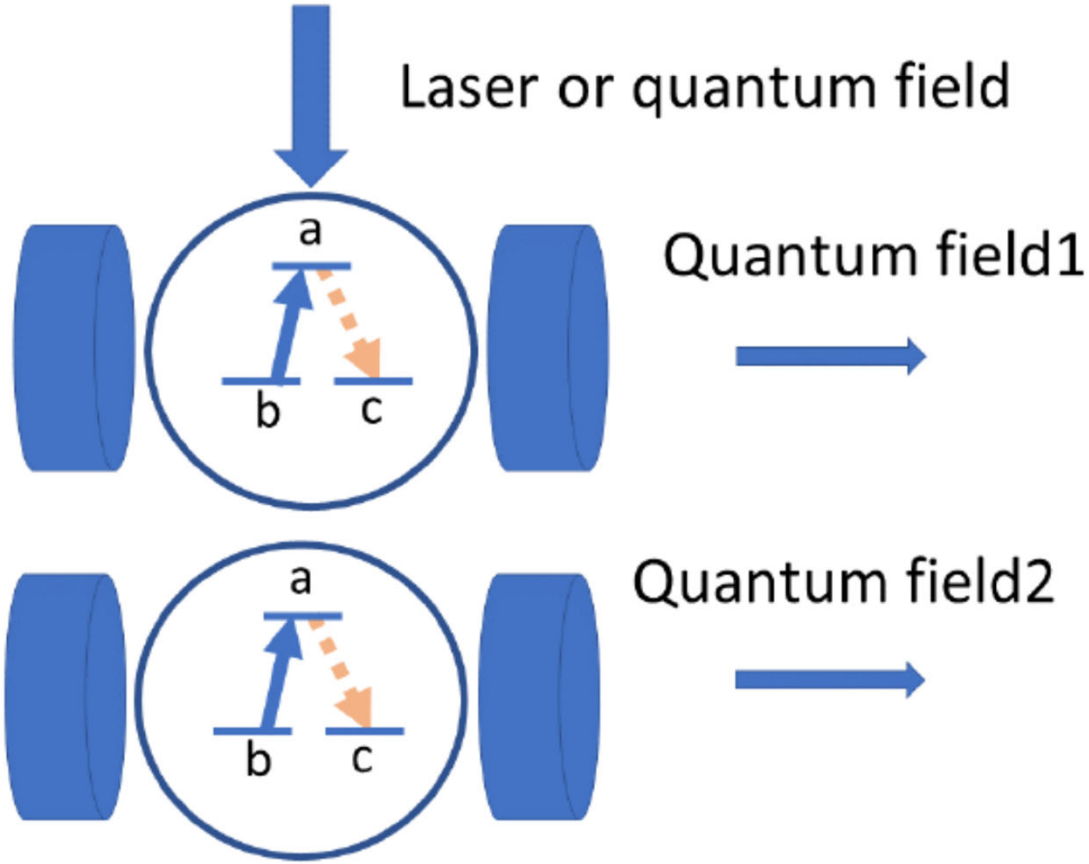

Jacob Emerick, et al., (2023).

Cooperative effects in metamaterials

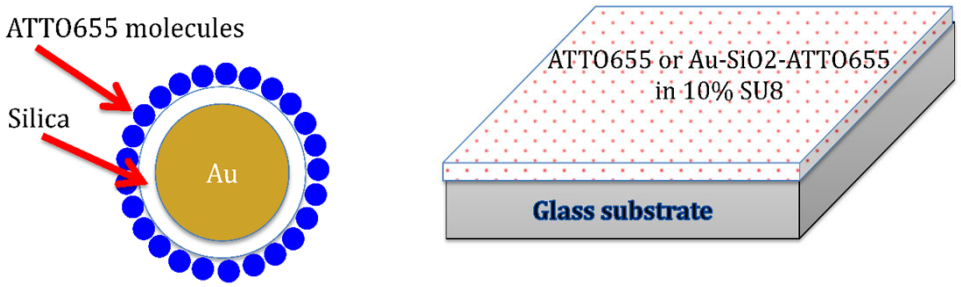

Fig. M2. A core-shell particle: diagram, scheme of deposition on a glass substrate.

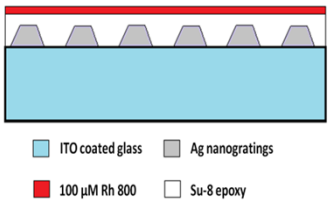

Fig. M1. A grating with SU-8 epoxy spacer 28nm, followed by Rh800 embedded in thinner epoxy 18 nm layer; gratings strips substructure: Ti 5nm, 30 nm Ag, 40 nm alumina, 5 nm Ti, 30 nm Ag, and 10 nm alumina. The periodicity of the gratings is ~310 nm. The e-beam writing parameters were as follows: dose was 650, 725, 750, and 800 μC/cm^2 for A, B, C, and D, respectively; 1.2 nA; and 100 kV accelerating voltage.

David P Lyvers, Mojtaba Moazzezi, Vashista C de Silva, Dean P Brown, Augustine M Urbas, Yuri Rostovtsev, Vladimir P Drachev, Cooperative bi-exponential decay of dye emission coupled via plasmons, *Journal Scientific Reports*, **2018**, 8. 9508.

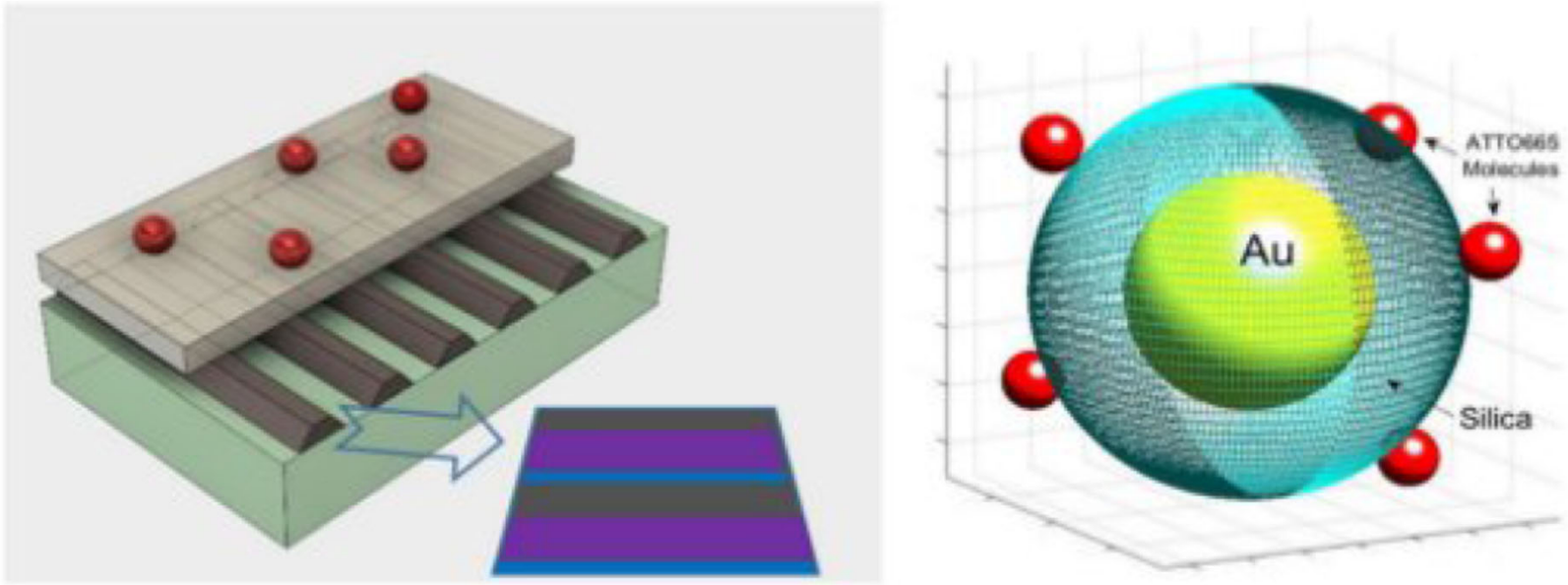

Figure 5: The models of the experimental and theoretical samples. Left - gratings with Rh800 molecules on top, grating strips substructure: Ti 5 nm (blue), 30 nm Ag (purple), 40 nm alumina (brown), 5 nm Ti (blue), 30 nm Ag (purple), and 10 nm alumina (brown). The periodicity of the gratings is 310 nm. Right Core shell nanoparticles Au/silica/ATTO655.

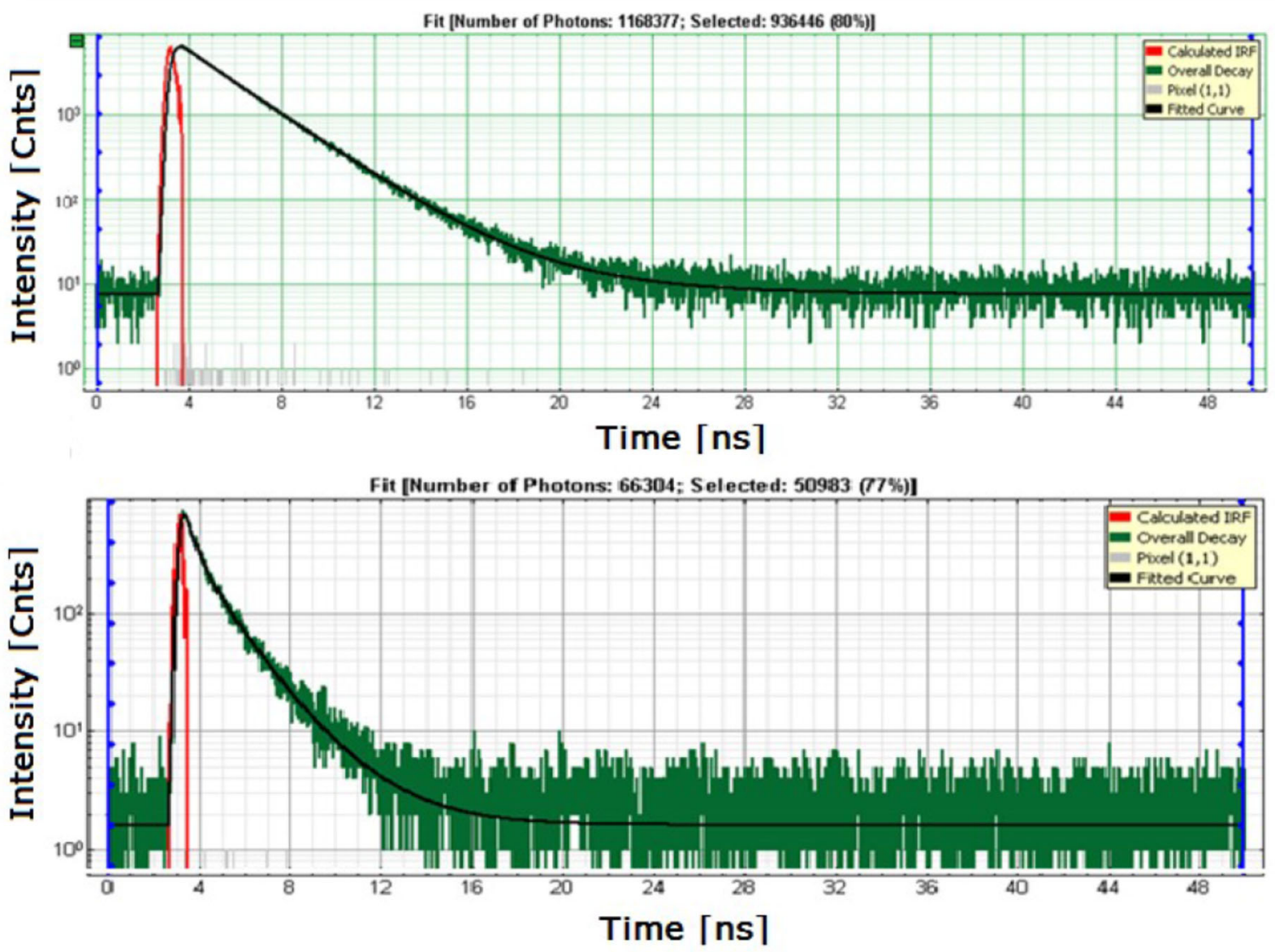
Fit [Number of Photons: 1168377; Selected: 936446 (80%)]
Calculated IRF
Overall Decay
Pixel (1,1)
Fitted Curve
Intensity [Cnts]
Time [ns]
Fit [Number of Photons: 66304; Selected: 50983 (77%)]
Calculated IRF
Overall Decay
Pixel (1,1)
Fitted Curve
Intensity [Cnts]
Time [ns]

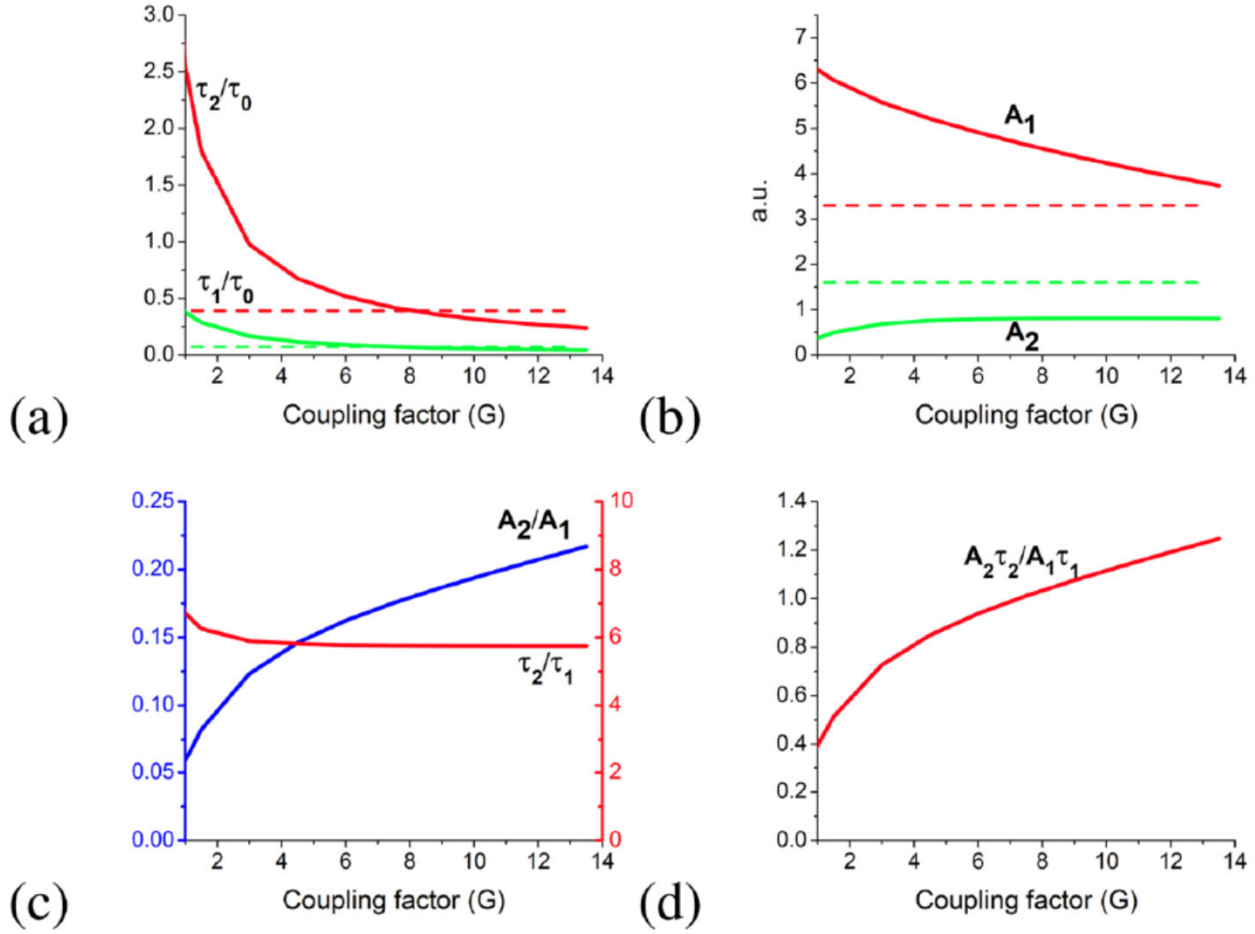

Figure 2. Bi-exponential fitting of theoretical results versus the effective coupling to the plasmonic structure. (**a**) The superradiance and subradience decay times τ_1 and τ_2 normalized by the decay time without metamaterial τ_0. Dashed lines show average of $A_1 e^{-t/\tau_1} + A_2 e^{-t/\tau_2}$ over $0 < G < 14$ (**b**) the amplitudes at the exponents A_1 and A_2, dashed lines are average. (**c**) A ratio of the amplitudes, and a ratio of the decay times, (**d**) a ratio of the total number of photons (a product of the amplitude and life time).

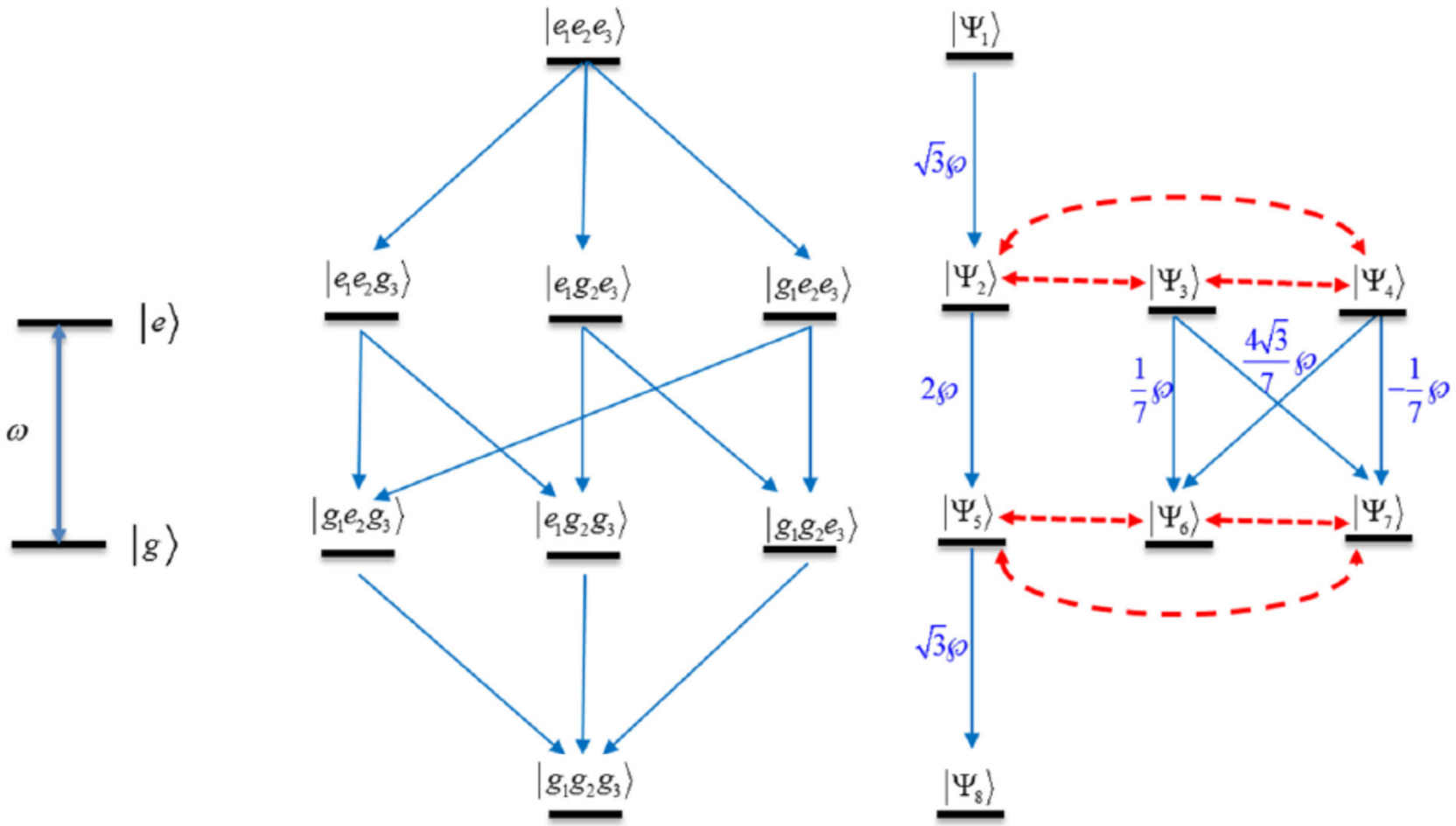

Figure 6. The scheme of energy level for the case of a single two -level atom (*Left*); the scheme of energy level for the case of three two-level atoms: (*Middle*) bare state basis and (*Right*) the Dicke state basis. The dipole-allowed transitions are shown by blue lines. The mixing between Dicke states are shown by the dashed red lines.

Blackbody radiation

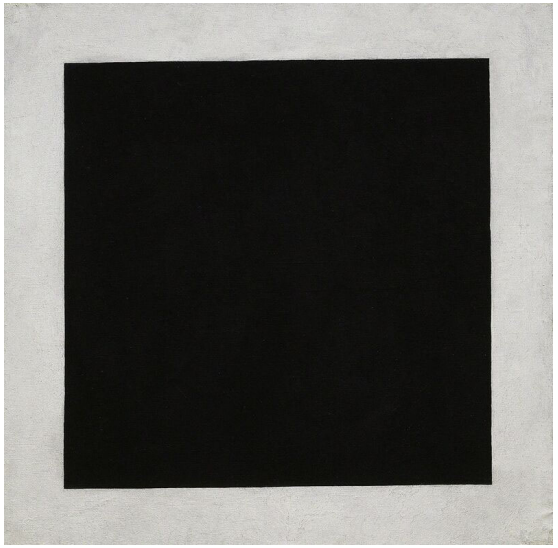

$$\mathrm{J}\omega = \frac{8\pi^2}{\lambda^4} \frac{\Delta\lambda}{\exp(\frac{hc}{k_B T\lambda}) - 1}$$

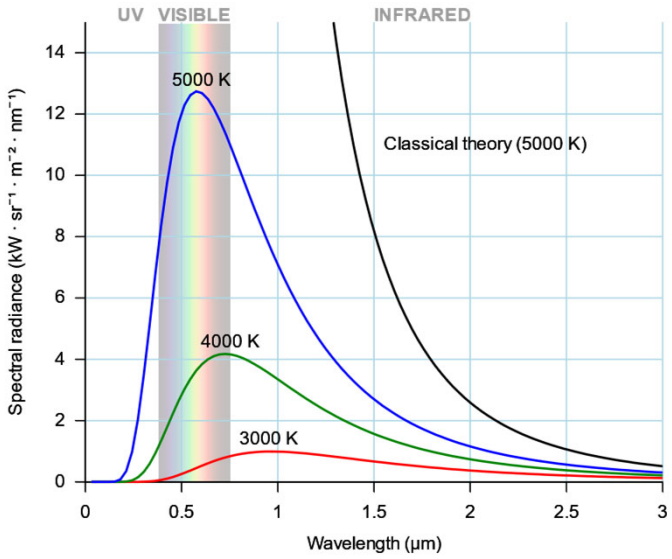

Biophotons vs blackbody radiation

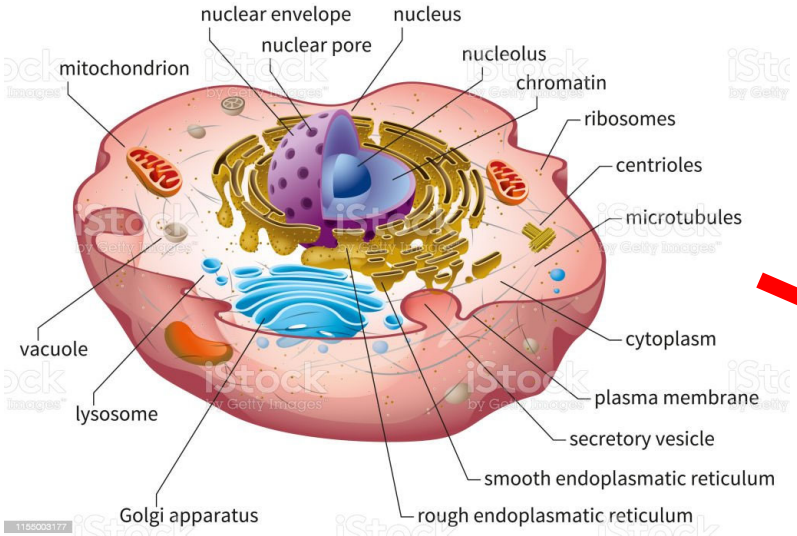

A living cell

A rock

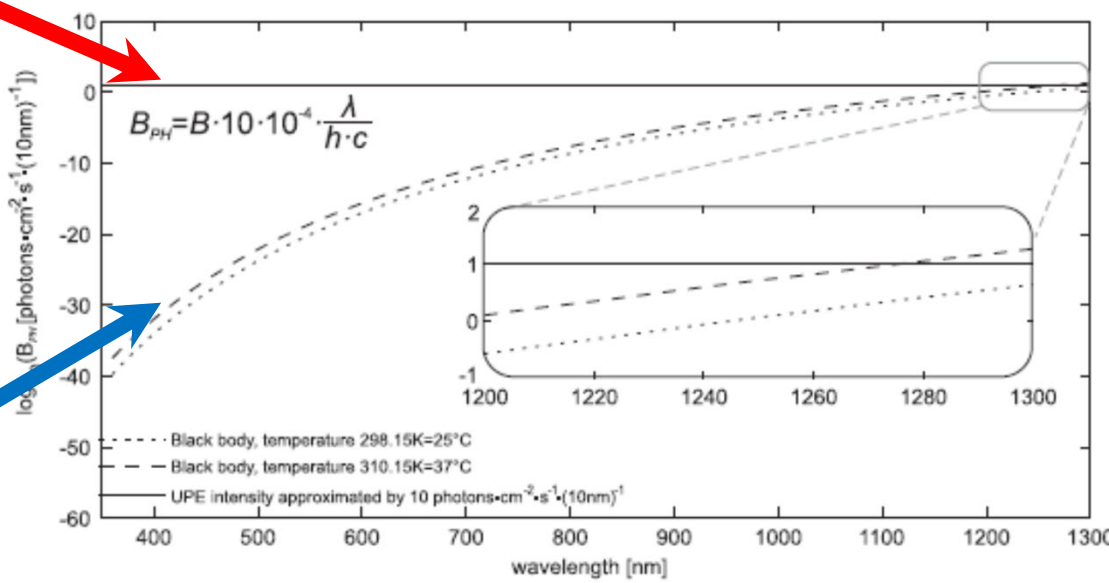

Biophotons, firefly

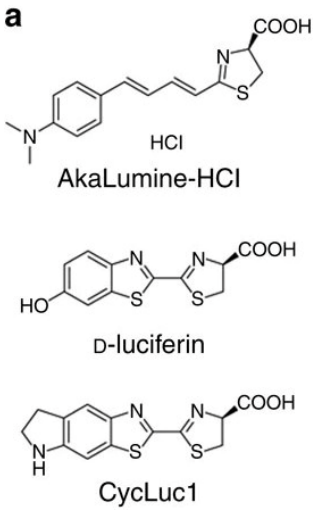

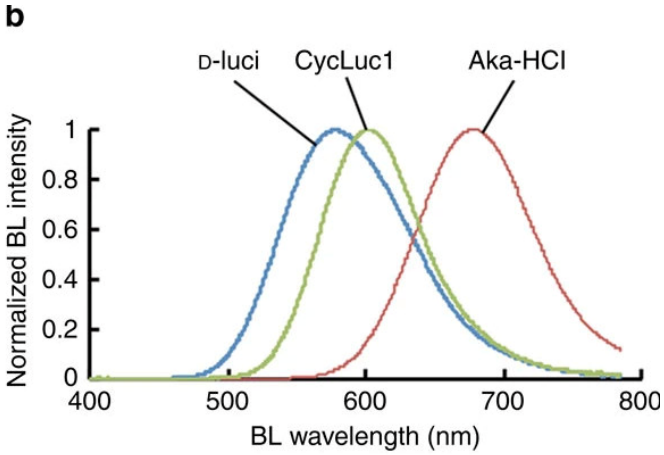

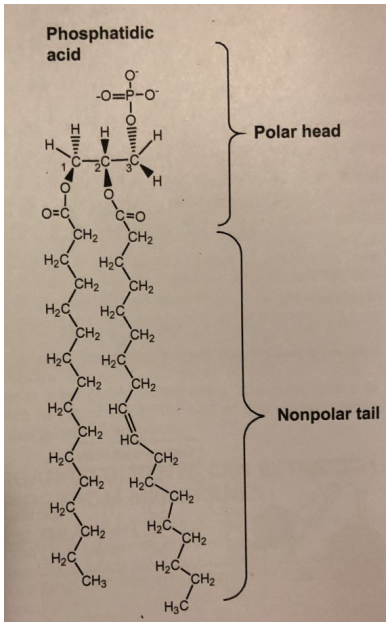
Phosphatidic acid
Polar head
Nonpolar tail

(A)

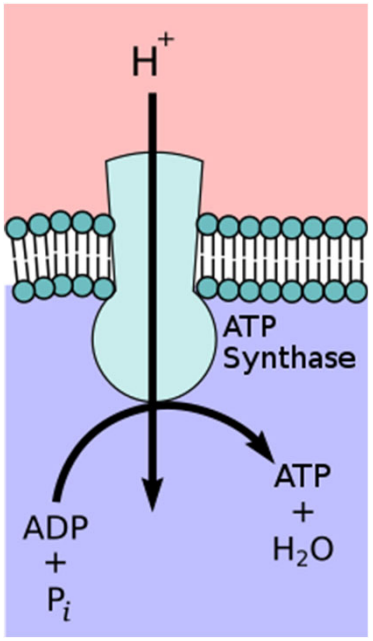
H+
ATP Synthase
ATP + H2O
ADP + Pi

(B)

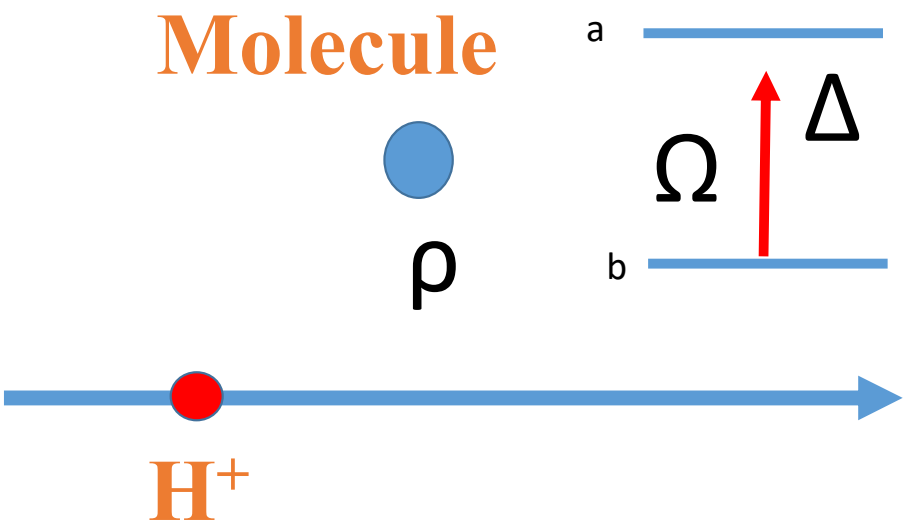
Molecule
a
Ω
Δ
b
ρ
H+

(C)

Biophotons

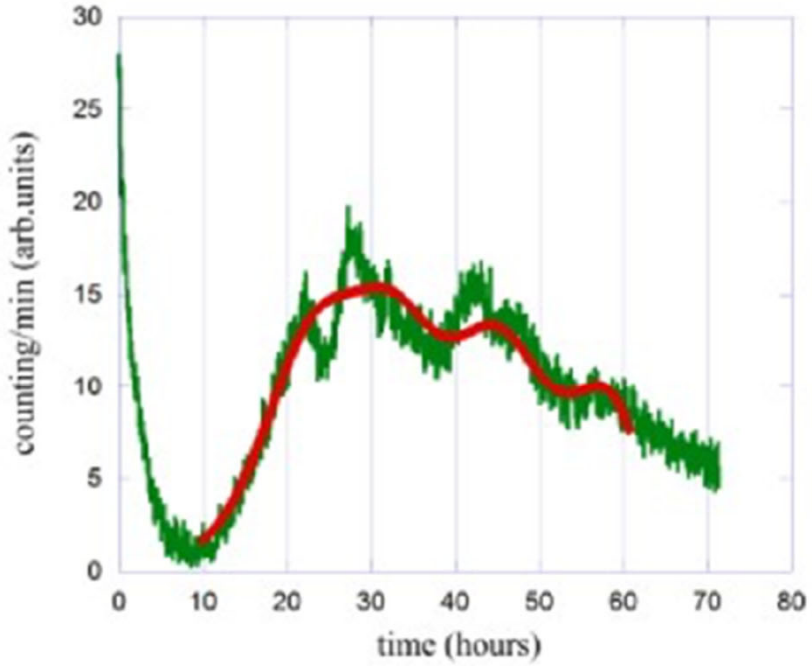

Figure 4: Comparison between the logistic equation prediction and experimental results of Ref. [42].

Biophotons

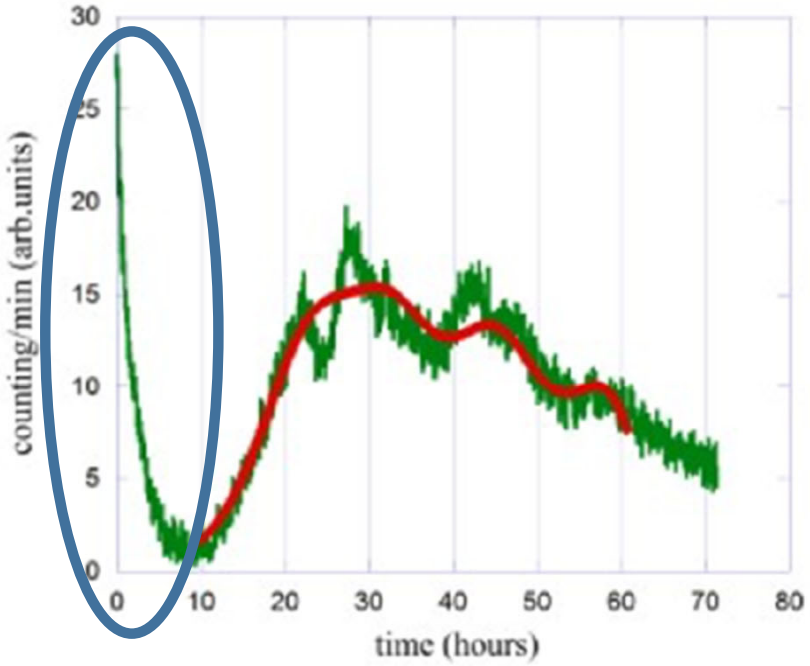

Figure 4: Comparison between the logistic equation prediction and experimental results of Ref. [42].

Biophotons

$$|B\rangle = \frac{\sum_{i=1}^{N} |bb...a_i...b\rangle}{\sqrt{N}}$$

$$|D_j\rangle = \frac{\sum_{i=2}^{j} |bb...a_i...b\rangle - (j-1)|bb...a_j...b\rangle}{\sqrt{j(j-1)}}$$

$$|B\rangle = \frac{|abbb\rangle + |babb\rangle + |bbab\rangle + |bbba\rangle}{\sqrt{4}}$$

$$|D_3\rangle = \frac{|abbb\rangle + |babb\rangle - 2|bbab\rangle}{\sqrt{6}}$$

$$|D_2\rangle = \frac{|abbb\rangle - |babb\rangle}{\sqrt{2}}$$

$$|D_4\rangle = \frac{|abbb\rangle + |babb\rangle + |bbab\rangle - 3|bbba\rangle}{\sqrt{12}}$$

$$\Gamma_{eff} \simeq \frac{1}{2}\left(\frac{\langle\delta\omega\rangle}{\Gamma_{col}}\right)^2 \gamma_{rad}$$

Conclusion

Properties of materials can be enhanced by the quantum coherent effects. We have shown that localized plasmon interaction in quantum confined structures strongly modify the optical and electronic properties with potential for manipulating light on the nanoscale.

- Transparency was observed in reduced graphene oxide near nanoparticles
- The molecular gas sensors based on adiabatic manipulation of the electric field have been experimentally demonstrated
- Manipulation of the absorption has been demonstrated in MoS2
- Ultra strong second harmonic generation has been shown in MoS2 promising the bright source of entanglement photons
- Control of the propagation of quantum fields using “quantum prisms”
- New area for quantum optics applications – quantum biology, biophotons, radiation produced by living tissues

We have demonstrated the quantum coherent effects are able to have an all-optical control, on ultrafast time scales, over the photonic topological transition, for applications as varied as quantum sensing, quantum information processing, and quantum simulations.

Thank you for your attention!

Thanks to my collaborators

Dr. Paolo Grigolini, Dr. Usha Philipose, Physics Department
Dr. Goran Brankovic, Dr. Zorica Brankovic, Belgrade University
Dr. Andrey Matsko, JPL
Dr. Anil Patnaik, AFIT
Dr. Gayatri Mehta, Department of Electrical Engineering
Dr. Kamesh Namuduri, Department of Electrical Engineering
Dr. Ione Hunt von Herbing, Department of Biological Sciences

PhD Students, Current

Colin Roy
MS. Mikaila Lapinski
MS. Steven Lanier
Erin Thornton
Trever Harborth
Brian Squires (together with Dr. Jingbiao Cui)
Cap Billi DeLuca (AFIT)
MS Charanaditya Padakandla Venkata (Department of Electrical Engineering)

Alumni

Dr. Abbas Goudarzi (2022)
Dr. Mojtaba Moazzezi (2018)
Dr. Pooja Singh (2016)
Dr. Suman Dhayal (2016)
Dr. Sankar Davuluri (2013)

Conclusion

Properties of materials can be enhanced by the quantum coherent effects. We have shown that localized plasmon interaction in quantum confined structures strongly modify the optical and electronic properties with potential for manipulating light on the nanoscale.

- Transparency was observed in reduced graphene oxide near nanoparticles
- The molecular gas sensors based on adiabatic manipulation of the electric field have been experimentally demonstrated
- Manipulation of the absorption has been demonstrated in MoS2
- Ultra strong second harmonic generation has been shown in MoS2 promising the bright source of entanglement photons
- Control of the propagation of quantum fields using “quantum prisms”
- New area for quantum optics applications – quantum biology, biophotons, radiation produced by living tissues

We have demonstrated the quantum coherent effects are able to have an all-optical control, on ultrafast time scales, over the photonic topological transition, for applications as varied as quantum sensing, quantum information processing, and quantum simulations.

Thank you for your attention!